

Electron-Driven *In Situ* Transmission Electron Microscopy of 2D Transition Metal Dichalcogenides and Their 2D Heterostructures

Rafael G. Mendes,^{†,‡,§} Jinbo Pang,[§] Alicja Bachmatiuk,^{†,§,⊥} Huy Quang Ta,^{†,‡} Liang Zhao,^{†,‡} Thomas Gemming,[§] Lei Fu,^{||} Zhongfan Liu,^{†,‡,¶} and Mark H. Rümmeli^{*,†,‡,§,⊥}

[†]Soochow Institute for Energy and Materials Innovations, College of Physics, Optoelectronics and Energy, Collaborative Innovation Center of Suzhou Nano Science and Technology, and [‡]Key Laboratory of Advanced Carbon Materials and Wearable Energy Technologies of Jiangsu Province, Soochow University, Suzhou 215006, China

[§]Leibniz Institute for Solid State and Materials Research Dresden, P.O. Box 270116, Dresden D-01171, Germany

[⊥]Centre of Polymer and Carbon Materials, Polish Academy of Sciences, M. Curie-Skłodowskiej 34, Zabrze 41-819, Poland

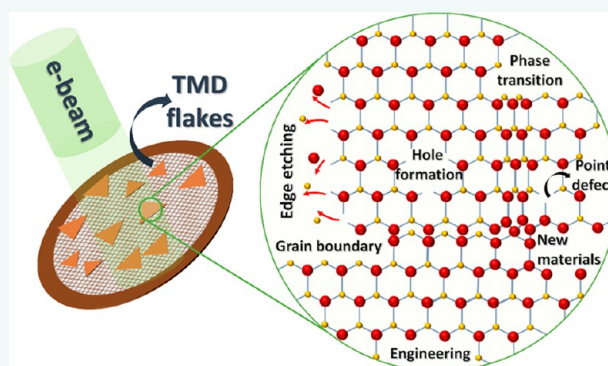
^{||}College of Chemistry and Molecular Science, Wuhan University, Wuhan 430072, China

[¶]Center for Nanochemistry, Beijing Science and Engineering Centre for Nanocarbons, Beijing National Laboratory for Molecular Sciences, College of Chemistry and Molecular Engineering, Peking University, Beijing 100871, China

ABSTRACT: Investigations on monolayered transition metal dichalcogenides (TMDs) and TMD heterostructures have been steadily increasing over the past years due to their potential application in a wide variety of fields such as microelectronics, sensors, batteries, solar cells, and supercapacitors, among others. The present work focuses on the characterization of TMDs using transmission electron microscopy, which allows not only static atomic resolution but also investigations into the dynamic behavior of atoms within such materials. Herein, we present a body of recent research from the various techniques available in the transmission electron microscope to structurally and analytically characterize layered TMDs and briefly compare the advantages of TEM with other characterization techniques.

Whereas both static and dynamic aspects are presented, special emphasis is given to studies on the electron-driven *in situ* dynamic aspects of these materials while under investigation in a transmission electron microscope. The collection of the presented results points to a future prospect where electron-driven nanomanipulation may be routinely used not only in the understanding of fundamental properties of TMDs but also in the electron beam engineering of nanocircuits and nanodevices.

KEYWORDS: monolayered materials, transition metal dichalcogenides, (scanning) transmission electron microscopy, *in situ*, heterostructures, electron beam engineering, electron-driven damage, nanomanipulation



The family of transition metal dichalcogenides (TMDs) has been known for many years. MoS₂ is the most studied family member and was first obtained in 1923.¹ TMDs are characterized by a weak and noncovalent bonding between their layers and strong in-plane covalent bonding, similar to graphene. Bulk TMDs can therefore be exfoliated to single or few layers.^{2–6} The isolation of a suspended MoS₂ monolayer was first achieved in 1986.⁷ This was driven by the discovery of graphene in 2004 by Novoselov and Geim⁸ after which our curiosity to find other single atom

and single unit cell thick two-dimensional (2D) materials started in earnest.^{9–19} Since then, the level of interest in TMDs has grown massively for both fundamental studies as well as their significant promise in numerous application areas such as microelectronics,^{20,21} batteries,^{22–24} solar cells,^{25,26} sensors,^{27–31} and biomedicine.^{32–34} TMDs comprise a metal

Received: October 22, 2018

Accepted: January 23, 2019

Published: January 23, 2019

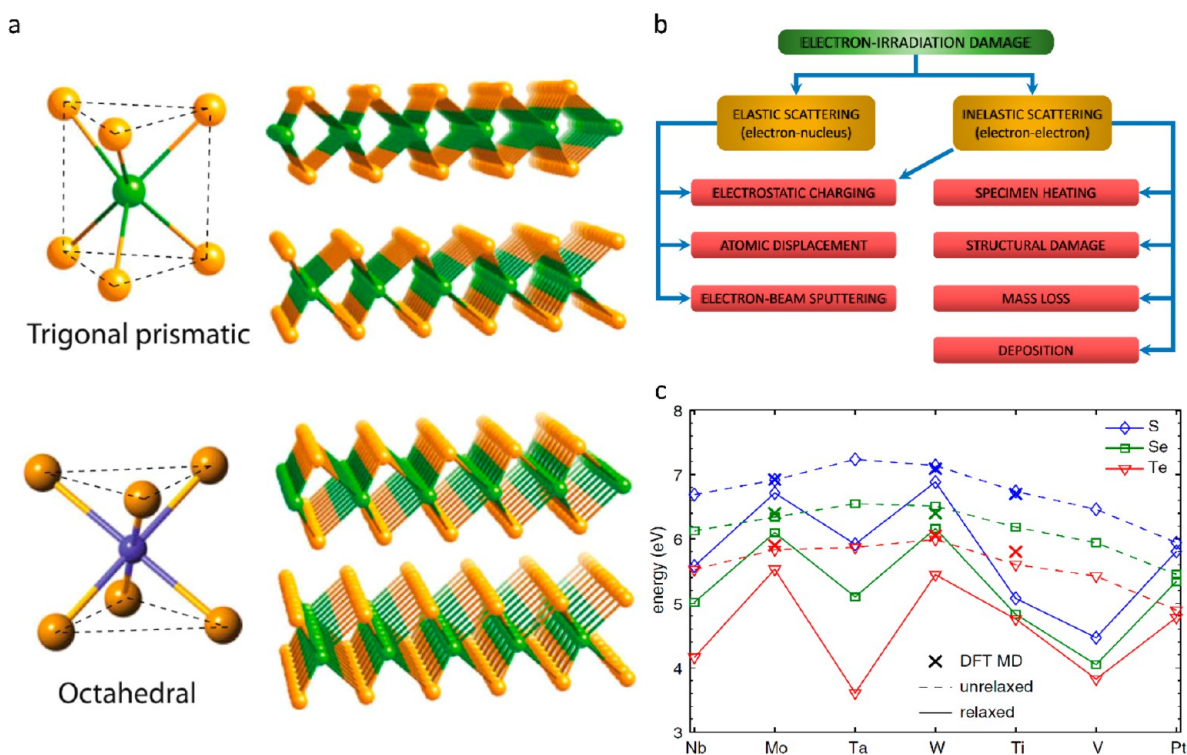


Figure 1. (a) Transition metal is represented by the green atoms and the chalcogen by the orange atoms. This atomic arrangement can form two types of crystals: (1) trigonal prismatic and (2) octahedral. Reproduced with permission from ref 35. Copyright 2016 Springer Publishing Group. (b) Radiation damage classification according to the type of electron scattering and according to the effects produced in a specimen. Reproduced and based on an image with permission from ref 67. Copyright 2004 Elsevier. (c) Displacement threshold energies obtained from DFT molecular dynamics calculations (crosses) and formation energies of chalcogen vacancies with nonrelaxed (dashed lines) and relaxed (solid lines) geometries in TMDs. Reproduced with permission from ref 80. Copyright 2012 American Physical Society.

layer sandwiched between two chalcogen layers.³⁵ As illustrated in Figure 1a, the plane containing the metal atoms is located between two planes of chalcogen atoms, forming a hexagonal arrangement, which can be trigonal prismatic or octahedral. In the trigonal prismatic crystal arrangement, the chalcogenides are stacked directly above each other, whereas in the octahedral crystal arrangement, they are staggered.³⁵

Monolayered MoS₂ and WS₂ are the most studied 2D TMD materials; however, there are many other 2D-layered materials with specific properties that are only recently attracting interest. Among the most exciting TMD family members to date are the semiconducting^{36–42} MoS₂ and WS₂ members, the WTe₂ and TiSe₂ semimetal members,^{43,44} and the true metal members,^{45–47} NbS₂ and VSe₂. There are also superconducting members,^{36–42} namely, NbSe₂ and TaS₂. It is not only single-layered TMDs that have great potential. The construction of hybrid TMDs, so-called heterostructures, in which different 2D materials are combined (stacked vertically or stitched laterally), is offering the opportunity for the design of truly man-made layered materials.^{48–51} The in-plane and out-of-plane stitching and stacking of different layered TMDs (and also in combination with other 2D materials) can render exhilarating properties and allow superior tuning for bespoke functionality.^{39,52–55}

Currently there is a need to both understand the fundamental properties of TMDs and design/modify TMDs using bottom-up approaches with the goal of precision tailored properties for application. To date, little is known about atomic defects and their effects on TMDs. Similarly, the effect of electron irradiation on TMDs is also relatively unknown.⁵⁶

Electron microscopy of TMDs offers a special possibility to investigate the fundamental properties of TMDs and study the interaction of an electron beam with the TMD lattice. Moreover, electron microscopy offers the potential to study TMDs^{57,58} and 2D materials, in general,^{59–64} with atomic precision and correlate their structure–property relationships. Hence, it is crucial to understand the interactions of electron irradiation on such specimens.⁶⁵ In transmission electron microscopes (TEM) and scanning TEM (STEM), the transmitted electrons, having interacted with the sample, are usually then collected to build an image of the sample or provide analytical information (e.g., electron energy loss spectroscopy (EELS) and energy-dispersive X-ray (EDX) spectroscopy). In addition, diffraction data can be extracted from the Fourier domain. To facilitate the understanding of the various TEM techniques covered in this review, a brief summary is presented in Table 1.

Modern TEM instruments allow one to obtain structural and spectroscopic information from samples at the atomic level, even at reduced acceleration voltages when spherical aberration (C_s) correctors are implemented. Electron beams with reduced energy distributions (cold field emission sources or monochromated sources) also help improve the obtained image resolution at low accelerations voltages (60 kV and below) where chromatic aberrations (C_c) become significant once the image has been C_s corrected.^{65,66} The potential to work with a broad electron energy window and maintain atomic level resolution is important not only for electron-beam-sensitive samples but also for electron-beam-driven engineering of materials, including TMDs.⁶⁵

Table 1. Brief Description of TEM Techniques Covered in the Review

TEM technique	brief description
scanning transmission electron microscopy (STEM)	This technique is a variation of TEM that uses a focused electron beam instead of a parallel beam that is scanned or rastered over a thin specimen. This technique allows the differentiation between different atomic elements due to differences in atomic mass. STEM also makes it possible to use analytical techniques such as EDX, EELS, and Z-contrast annular dark-field (ADF) imaging at a local scale.
selected area electron diffraction (SAED)	Diffraction is an indispensable technique often used in TEM to unravel crystal-symmetry information on small areas of the sample. For this, the usual parallel TEM beam is focused, which produces a convergent beam. In order to more precisely select the area of interest as well as reduce the intensity of the beam reaching the sample, a set of apertures with different sizes can be used. In this case the measurement is called selected area electron diffraction (SAED).
electron energy-loss spectroscopy (EELS)	This refers to an analytical tool that is related with the kinetic energy of electrons after they interact with a thin specimen. This allows the determination of the energy distribution of electrons that pass inelastically, losing energy, through the specimen. EELS provides therefore an immense amount of information about the chemistry and electronic structure of atoms, which in turn is related with bonding and valence states, nearest atomic environment, dielectric response, free-electron density and band gap.
energy-dispersive X-ray spectroscopy (EDX)	This is another analytical technique available in TEM used for elemental analysis of a sample. In order to generate the X-ray from the sample, the high energy electron beam interacts with the sample, which excites an electron in the inner shell of the atomic shell, ejecting it from the shell. In the process of an electron from an outer shell occupying the hole, an X-ray is emitted from the specimen and can be detected. As the energies of the X-ray are specific to the energy levels of the atom/s in question, it is possible to investigate the elemental composition of the measured sample.

Electrons from the imaging beam in a TEM undergo elastic and inelastic electron interactions with the specimen (*e.g.*, TMD) which can lead the specimen heating, charging, ionization damage (radiolysis), atom displacement damage (knock-on damage or sputtering), or electron-beam-induced carbon deposition from hydrocarbon contamination.^{65,67–73} Figure 1b summarizes the main types of electron irradiation effects/damage.

The most relevant electron-beam-induced processes on 2D materials can be narrowed down to knock-on damage and radiolysis. Knock-on damage is an elastic electron–specimen interaction that has a threshold energy above which the atomic displacement occurs and is dependent on the material in question due to its bond strength, crystal lattice, and atomic weight of the atoms forming the structure. Hence, the choice of accelerating voltage is important as the only way to avoid knock-on damage is to use an incident energy below the threshold energy. Radiolysis can be understood as electron-beam-induced sample degradation through inelastic scattering producing atomic displacements, which leads to loss of crystallinity and/or mass loss. Radiolysis is somewhat dependent on temperature and can be reduced by cooling the sample.^{65,67}

Recently, significant attention has been given to the development of *in situ* TEM, aiming to unravel atom by atom the dynamic processes involved in the synthesis of materials as well as understand the electron beam and sample interactions.⁷⁴ This allows investigation of lattice dislocations, point defects, grain boundaries, and phase transition. In addition, *in situ* TEM offers us tantalizing ways to engineer 2D materials and heterostructures with atomic precision. Scanning transmission electron microscopy has also been used extensively with high spatial and temporal resolution. Since contrast in STEM imaging is intrinsically related to the atomic weight (so-called Z-contrast), it is possible to track specific elements in the lattice under investigation. On the other hand, as image capture in TEM is collected with a near parallel electron beam, TEM offers superior temporal resolution as compared to STEM.

Herein, we review the latest research performed using TEM and STEM to understand both the structural aspects of TMDs and the dynamics of atom rearrangement due to electron-beam-induced interactions or transformations such as phase transitions as well as the synthesis of other TMD-based nanomaterials.

TRANSFER APPROACHES FOR TEM INVESTIGATIONS

The transfer of 2D materials from a substrate to a TEM grid is the first step toward the successful imaging and characterization of TMDs. To date, transfer techniques remain a challenge due to sample degradation and contamination that are difficult to avoid during the transfer process. However, with care and patience, suitable samples can be prepared and imaged successfully. It is important to mention that high-resolution TEM imaging (as well as for other techniques) represents only a very small fraction of the sample. It is also very common and often omitted that the results published depict the cleanest and best situation to illustrate the phenomena being studied. Although the reproduction in sample preparation is in most cases achieved and the problem of contamination can be addressed for the purposes of high-resolution imaging, it is still a challenge to have samples without any contamination distributed across the surface of the

specimen. Therefore, we want to point out that the transfer techniques described in this review are good solutions to allow successful high-resolution images but do not represent the final solution to remove contaminants completely. In this section, we briefly look at the most relevant transfer techniques of TMD films or flakes onto TEM grids. As a general rule, transfer from a substrate to a TEM grid can be done in five basic steps: (1) synthesis of TMD on a substrate, (2) coating of a substrate with a poly(methyl methacrylate) (PMMA) capping layer, (3) detaching of TMD embedded in the PMMA capping layer, (4) placing the PMMA capping layer containing the TMD flakes onto the TEM grid, and (5) dissolving the PMMA capping layer so the TMD flakes remain on the grid.

Currently, the most commonly used transfer approach for TMDs involves wet-etching, which is similar to that often implemented for graphene.⁷⁵ In this approach, the substrate containing the TMD is coated with a support film of PMMA. The substrate is then chemically etched, and the TMD embedded in the PMMA film can be removed. The film is then placed onto a TEM grid with an amorphous holey carbon film, and the PMMA is dissolved away using a solvent in liquid or hot vapor form. As a result, the TMD remains attached to the grid and can be characterized. Mlack *et al.*⁷⁶ demonstrated the transfer of WS₂ grown on SiO₂ by using the PMMA method. Etching the substrate was achieved using KOH so as to detach the PMMA–WS₂ film prior to transfer.

A chemical etching-free transfer referred to as ultrasonic bubbling transfer has also been reported by Ma *et al.*⁷⁷ In their method, a PMMA-coated substrate containing MoS₂ film is immersed in water and ultrasonicated. The ultrasonication generates micron-sized cavitation bubbles. During the collapse of the bubbles, the forces generated at the interface between the PMMA-capped MoS₂ and the substrate are enough to detach the PMMA-capped MoS₂. This process does not use any chemicals and is referred to as a physical exfoliation process.

After the successful transfer of the layered TMD onto a TEM grid, numerous techniques can be performed using TEM to characterize the material both structurally and analytically. Conventional TEM imaging is the most routine method together with SAED to obtain structural information from the material. However, high-resolution STEM imaging has gained a lot of attention, due to its ability to provide not only structural information but also chemical information through Z-contrast, as mentioned above. This is of particular interest when studying heterostructures and doped layers, as the position and distribution of the different atoms is required in order to tune specific and desired properties. To further confirm the chemical composition of the investigated material, it is also possible to perform EELS and EDX mapping of the region of interest. This provides incredibly detailed and useful information about the atomic distribution of atoms, heterojunctions, and layers.

Detailed atomic and chemical information can be obtained using STEM as shown by Dumcenco *et al.*⁷⁸ They obtained statistics of the atomic distribution of Mo and W under different conditions with incredible precision. For each of the conditions, EDX and ADF measurements were performed and showed how one can detect an increase in W content by changing the initial chemical conditions within the CVD synthesis reaction.

DYNAMIC *IN SITU* TEM OF TMDs

Typically, 2D materials are sensitive to electron beam irradiation. This means that damage to the crystalline structure can easily occur during image collection. The simplest way of studying the interaction of electron beam with TMD is to simply irradiate the sample and record the irradiation damage with respect to time. We believe that the understanding of the processes involved in electron-driven modification of materials and the possibility of tailoring the properties of materials with an electron beam together with developments in artificial intelligence and automation at the nanoscale will contribute to push forward the field toward the creation of highly advanced electron beam engineering technology. Herein, we present studies on point defects, grain boundaries and production of nanoribbons and nanowires and TMDs that support the idea of a possible future where electron beam can be used a craft tool to enable to design of nanocircuits and nanodevices with TMDs.

Most studies on TMD defects thus far have been conducted with exfoliated MoS₂. Park *et al.*⁷⁹ described how defects can be created on the most common polymorph, 2H MoS₂. The hole formation on MoS₂ was achieved by removing either one molybdenum (Mo) atom or two sulfur (S) atoms. However, the number of holes created by the removal of sulfur is higher due to the lower knock-on damage threshold energy. It is thought that, at the edges of a hole, Mo agglomerates due to its the high knock-on threshold, whereas sulfur is easily ejected. According to the literature, S has a knock-on threshold energy of 80 kV and Mo a value of 560 kV.⁸⁰

Atomic defects can significantly affect the physical and chemical properties of nanomaterials. Therefore, to avoid electron-induced damage, it is preferable to have an understanding of some of the intrinsic properties of the material to be investigated. This includes knowing the knock-on energy threshold prior to the measurement. Komsa *et al.*⁸⁰ employed first-principles simulations to study the behavior of 21 TMD compounds under electron irradiation and calculated the knock-on threshold energies for each. For the theoretical calculations they relied on density functional theory (DFT) implementing the Perdew–Burke–Ernzerhof exchange–correlation function.⁸¹ DFT molecular dynamics were used to calculate the displacement threshold energy T_d (minimum initial kinetic energy of the recoil atom) until it was high enough to displace an atom from its lattice. This results in the formation of a vacancy. These values were compared with the nonrelaxed and relaxed vacancy formation energies E_f . The calculated results are presented in Figure 1c.

Electron-beam-induced damage on the lattice of TMDs can also lead to the formation of innovative materials. Liu *et al.*⁷⁴ highlights in detail dynamic *in situ* TEM on the manipulation and formation of such a material in which layered MoS₂ serves as the precursor material. Their work demonstrated a different approach to fabricate uniform and robust semiconducting molybdenum-sulfide ribbons. To accomplish this, they used electron beam irradiation at the edge of a MoS₂ sheet to produce holes that spread quickly and produce a ribbon between them. A phase transition occurs when the ribbon reaches a critical size below 1 nm, forming a robust Mo₃S₄ structure.

The work from Lin *et al.*⁸² demonstrates that it is possible to fabricate TMDs nanowires using a focused electron beam. They used a focused low-energy electron beam operating at 60

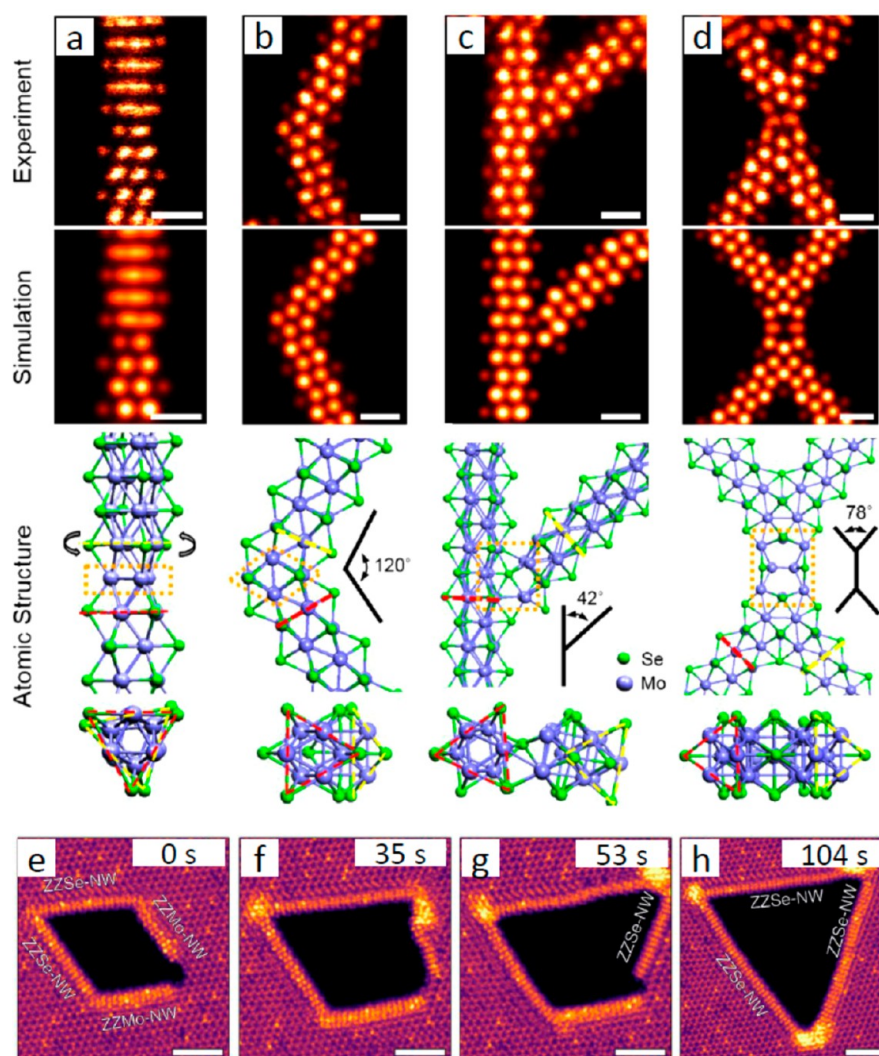


Figure 2. (a–d) Structural flexibility of MoSe nanowires. The experimental Z-contrast STEM images are shown in first row, the corresponding simulated STEM-ADF images are shown in the second row, and the top and side views of the atomic models are shown in the third row. (a) Large twist in MoSe nanowire; (b) kink which changes the axial direction; (c) branch where another MoSe nanowire protrudes from the original direction forming a Y junction, and (d) X junction which connects four MoSe nanowires. (e–h) Shape evolution of an etched pore with all edges terminated by nanowires. Scale bars are 2 nm. Panels (a–d) reproduced from ref 83. Copyright 2016 American Chemical Society. Panels (e–h) reproduced with permission from ref 84. Copyright 2018 Nature Publishing Group.

kV to produce nanowires from MoSe₂ and MoS₂ monolayers. The nanowires were formed by creating two holes side by side using a focused electron beam leaving a central ribbon, which was then etched by electron irradiation. This process can be done in different areas of the TMD lattice to form nanowire networks and Y junctions. The length of the nanowires and nanojunctions can be determined by the size of the initial ribbon and is self-regulated most probably by spontaneous phase transition triggered by the electron irradiation. The direct manipulation of TMD nanowires at the atomic level using a controlled focused electron beam in STEM mode was also demonstrated by Lin *et al.*⁸³ They reported the possibility to regulate the chemical constitution and flexibility of TMD nanowires as well as form complex junction arrangements, as shown in Figure 2a–d with different properties that can be used in future nanodevices.

Recently, Sang *et al.*⁸⁴ also reported the formation of nanowires on the edge of holes in TMD by monitoring the evolution of pores in Mo_{1-x}W_xSe₂ monolayers. They

accomplished this by using an electron beam operating at 100 kV and collecting a series of aberration-corrected STEM images as shown in Figure 2e–h. It is important to mention that in their work electron irradiation and heat were used to trigger the hole evolution. The etching kinetics of the holes is determined by the edge-termination of the hole. Se-terminated edges are prone to etch fast and along a lateral direction, whereas the nanowire-terminated edges etch along a longitudinal direction. The ability to controllably etch TMD layers with an electron beam offers the possibility to predictably control the electrical and magnetic properties of TMDs and their incorporation in nanostructured devices.⁸⁴

Electron-beam-driven defects, dislocations, and grain boundaries in TMD crystals can also have a significant effect on their properties. Point defects, dislocations, and grain boundaries can introduce states in the band gap of a material affecting the Fermi level and properties of semiconductors.^{85–89} Hong *et al.*⁹⁰ investigated defects in MoS₂ films produced by mechanical exfoliation, physical and chemical

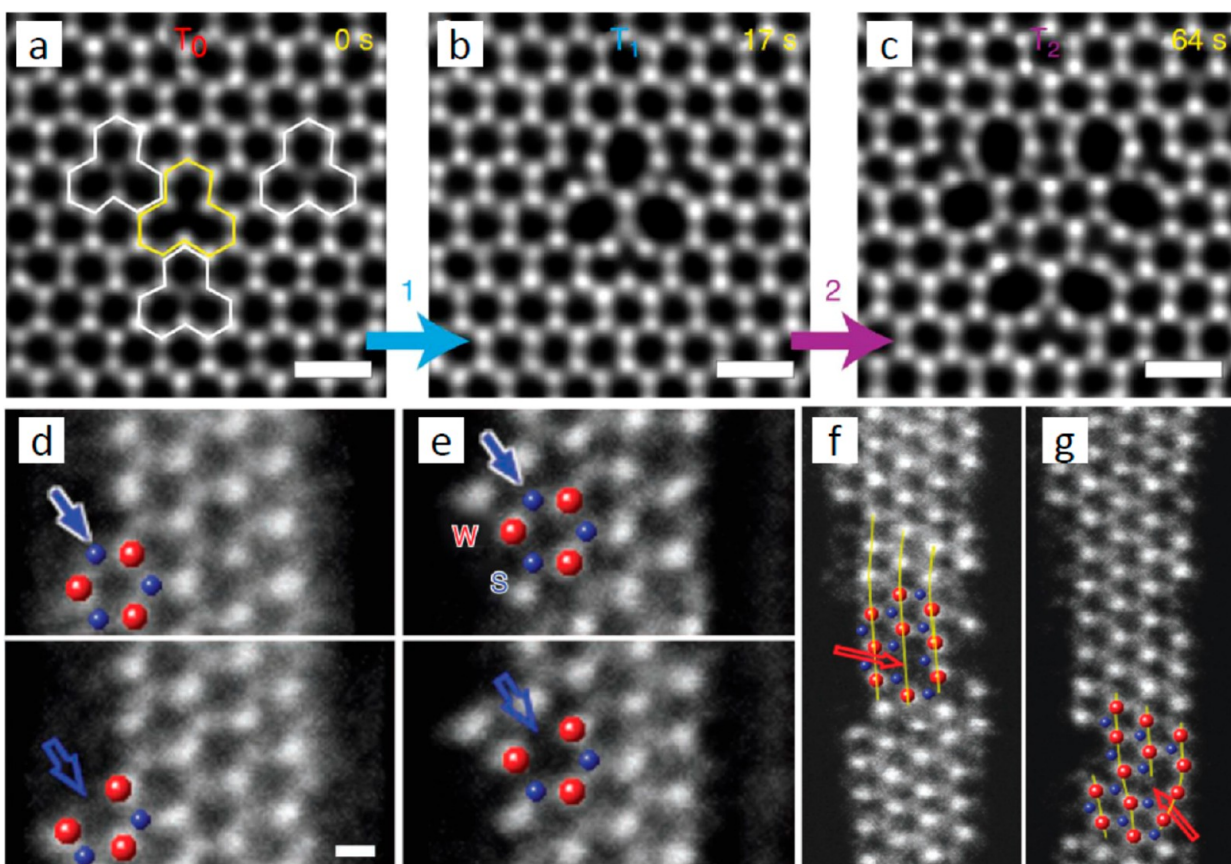


Figure 3. (a–c) Formation and evolution of rotational defects in WSe₂ monolayers. Scale bar is 0.5 nm. (d–g) Single atomic defect in a monolayered WS₂ nanoribbon. (d,e) Dynamic process of the atomic defects created at S sites. (d) Edge-atom loss of S and (e) vacancy created. (f) Simple W monovacancy and (g) W vacancy with a large distortion in the surrounding lattice. The open blue arrows indicate the loss of S atoms, and the red open arrows indicate the W vacancies. Scale bar is 0.2 nm. Panels (a–c) reproduced with permission from ref 106. Copyright 2015 Nature Publishing Group. Panels (d–g) reproduced with permission from ref 107. Copyright 2011 Nature Publishing Group.

vapor deposition. The density of defects was characterized using STEM as well as *ab initio* calculations. They could correlate the type of defects and the local change in electric and magnetic properties of the MoS₂ monolayer. Defects are also a controlling factor in the optical properties of 2D materials.^{91–95} Lin *et al.*⁹⁶ investigated the influence of defects and dopants on the photoluminescence of WS₂ films. This was achieved by combining both imaging (STEM) and spectroscopy (EELS) and correlating those with the photoluminescence of different WS₂ flakes. The production of individual nanotriangles within the WS₂ lattice could possibly increase the efficiency of light emission. It is crucial to mention that such defects can be controllably created using an electron beam, reinforcing the importance of electron beam engineering of 2D materials.⁵⁶ Edelberg *et al.*⁹⁷ also describe the increase of light emission in MoSe₂ and WSe₂ films due to the nature of point defects found in the lattice.

Point defects and dislocations can also create deformation sites, especially when subjected to stress, which are highly reactive regions making them suitable for atom substitution^{98–101} or functionalization,³⁵ which are also methods to tailor electronic and optical properties of 2D materials and their heterostructures. Li *et al.*¹⁰² described that the Se/S substitution rate in MoS₂ gradually decreases from the edge toward the center of the lattice, which can be explained by a

strain-driven substitution mechanism. This mechanism might be of relevance in other TMDs and 2D nanostructures.

Atomically resolved images depicting single atom displacements and vacancies combined with first-principles calculations are one of the most promising techniques to study defects in materials. Zhou *et al.*¹⁰³ looked at point defects in CVD-grown MoS₂ films using STEM-ADF imaging. They showed the presence of six basic point defects, which includes a monosulfur vacancy (V_S), a disulfur vacancy (V_{S2}), a vacancy complex of Mo nearby three sulfur pairs (V_{MoS3}), a vacancy complex of Mo nearby three disulfur pairs (V_{MoS6}), and anti-site defects where a Mo atom substitutes an S₂ column (Mo_{S2}) or an S₂ column substituting a Mo atom (S₂Mo). Their study also revealed that electron beam energies below the knock-on threshold energy could also lead to damage with long exposure times. They determined that the preferred defects generated by extended electron beam irradiation are the V_S and V_{MoS3} defect types. Similar point vacancies imaging and theoretical studies on TMDs have also been published.^{104,105}

Lin *et al.*¹⁰⁶ investigated formation and evolution of rotational defects caused by chalcogen vacancies driven by the interaction of the electron beam with WSe₂ monolayers. Figure 3a–c shows STEM images of Se-deficient areas. The presented images show the evolution of the defects at intervals of 64 s. They claim that such rotational defects are different from those

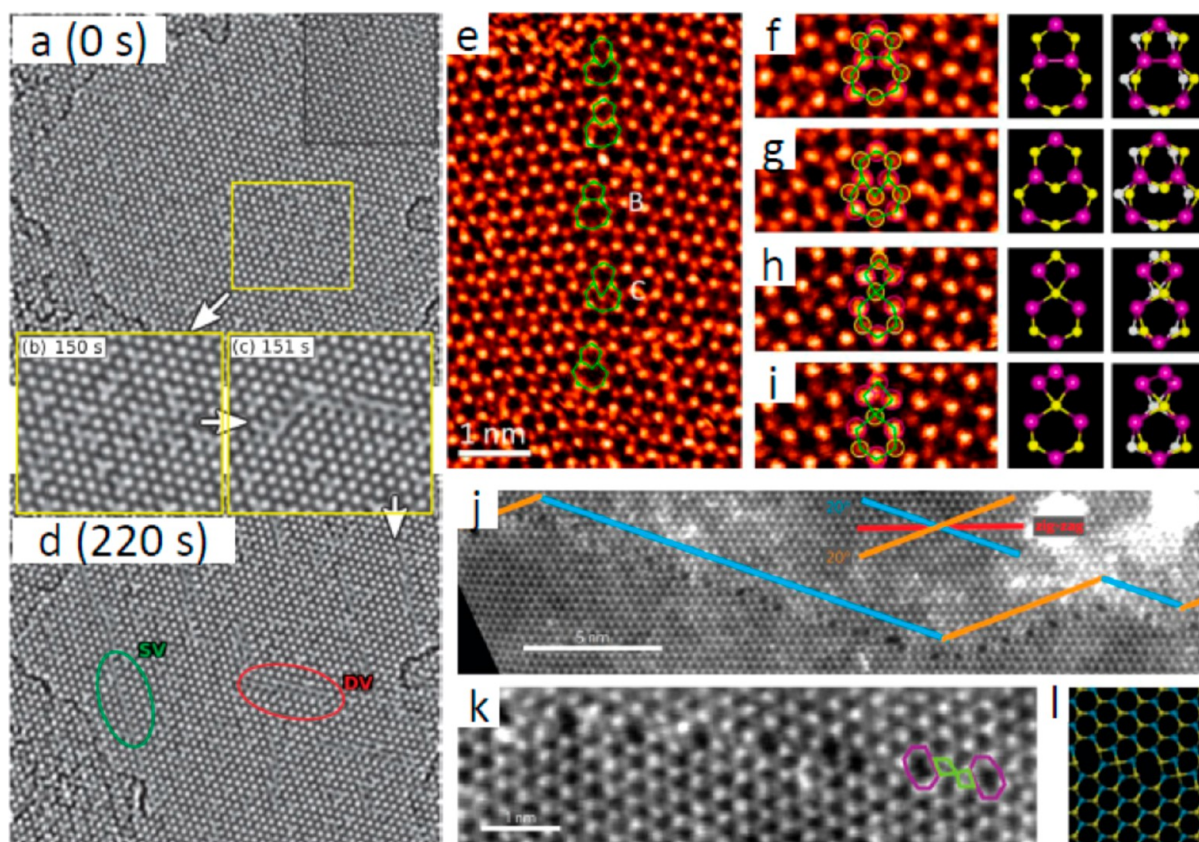


Figure 4. High-resolution TEM images showing the formation of line defects under electron irradiation at 80 kV. (a) Initial configuration with a certain number of S vacancies already present. (b,c) Intermediate configurations illustrating formation of defect lines through agglomeration of nearby vacancies. (d) Final configuration after 220 s, where a large number of defect lines can be seen. Examples of single-vacancy (SV) and double-vacancy (DV) lines are highlighted. The shape of the DV line as changed from that shown in (c). HRTEM frames are low-pass-filtered to reduce Poisson noise. An unprocessed region is shown in the upper-right corner of (a). (e–i) Atomic structure of small-angle grain boundaries in monolayer MoS₂. (e–g) STEM-ADF images of an 18.5° grain boundary consisting of dislocations with five- and seven- (5/7) and dislocations with six- and eight-fold rings (6/8). Panels (f) and (g) are the zoom-in view of the 5/7 and 6/8 structures from the regions indicated in (e). (h,i) ADF images of a 17.5° grain boundary consisting of dislocations with four- and six-fold rings (4/6) rings, either pristine shown in panel (h) or with Mo substitution shown in panel (i). The 2D and 3D structural models for the various dislocation structures are placed next to the corresponding ADF images. (j–l). Grain boundary atomic structure. (j) High-resolution ADF-STEM image of a mirror twin boundary. The boundary is visible just below the annotated line. The annotation indicates the nanoscale faceting of the boundary at $\pm 20^\circ$ off of the zigzag direction. (k). Zoomed-in image of the grain boundary shows a periodic line of 8–4–4 ring defects. (l) Atomistic model of the experimental structure shown in (b). Panels (a–d) reproduced with permission from ref 108. Copyright 2013 American Physical Society. Panels (e–i) reproduced from ref 103. Copyright 2013 American Chemical Society. Panels (j–l) reproduced with permission from ref 117. Copyright 2013 Nature Publishing Group.

observed in other 2D materials and that this type of defects may lead to significant changes of the materials properties.

Point defects were also investigated by Liu *et al.*¹⁰⁷ with a monolayer WS₂ film using time-resolved ADF imaging to discriminate single atom defects on WS₂ nanoribbons. The point defects created in the WS₂ lattice were induced by increasing the beam current (not energy) and the dynamic interactions between the electron beam and specimen, leading to atomic defects (vacancies) were observed and recorded. They found individual S and W vacancies and determined that S vacancies do not induce large distortions in the nanoribbon. However, W vacancies induce a rather drastic structural deformation in the WS₂ nanoribbon lattice as shown in Figure 3d–g.

Further studies conducted to determine the evolution of defects on monolayer MoS₂ films under electron beam irradiation were conducted by Komsa *et al.*¹⁰⁸ They used an electron beam with an accelerating voltage of 80 kV and irradiated the MoS₂ film for up to 220 s while recording

changes to the lattice. As mentioned above, they also studied pre-existing defects, presumably created during synthesis or the sample transfer process. Upon exposing the material to the electron beam, additional point vacancies were continuously produced and shown to diffuse along the lattice at a slow rate. As the number of vacancy sites increased, extended line defects could be observed to form and continue elongating, as shown in Figure 4a–d. This leads to a final structure that is significantly different from the initial material.

Grain boundaries (GBs) and dislocations in TMDs have also been studied. A first-principle theoretical study¹⁰⁹ predicts that the structure of dislocations and their formation into GBs is very complex and intrinsically dependent on the type of dislocation and constituent elements of the TMD in question. The synthesis of large-area 2D materials leads inevitably to the production of randomly oriented GBs,^{110–112} causing changes in the properties of the material. The control over the atomic structure of GBs is important to tailor properties of low-dimensional material especially concerning the electrical

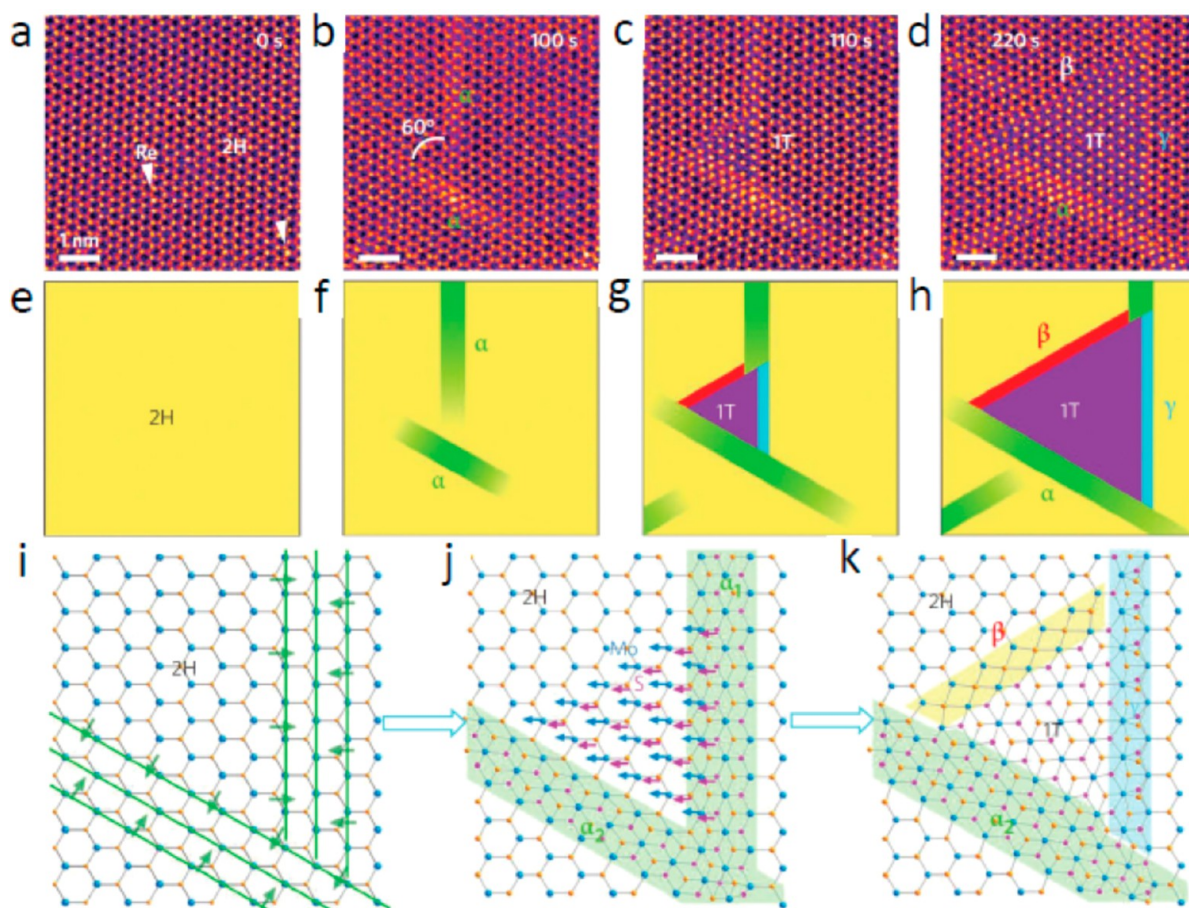


Figure 5. (a) Single-layered MoS₂ doped with Re substitution dopants (indicated by arrowheads) has the initial 2H phase of a hexagonal lattice structure with a clear honeycomb structure. (b) At $t = 100$ s, two identical intermediate (precursor) phases (denoted α) form with an angle of 60° and consist of three constricted Mo zigzag chains. (c) At $t = 110$ s, a triangular shape indicating the 1T phase (~ 1.08 nm²) appears at the acute corner between the two α -phases. (d) At $t = 220$ s, the area of the transformed 1T phase is enlarged to ~ 8.47 nm². Three different boundaries (α , β , and γ) are found at the three edges between the 1T and 2H phases. (e–h) Simple schematic illustrations of the 2H \rightarrow 1T phase transition corresponding to the ADF images in (a–d), respectively. (i) Atomic model of α -phase formation by the constriction of three Mo zigzag chains. (j) Nucleation of the 1T phase (triangular) with the Mo + S (or S') atoms gliding in the directions indicated by the blue and pink arrows. (k) β -Boundary formation at the growth frontier side. Panels (a–k) reproduced with permission from ref 128. Copyright 2014 Nature Publishing Group.

transport capabilities.^{113,114} Therefore, atomic investigation and local engineering of GBs is essential to understand and design materials with the desired properties. Zhou *et al.*¹¹⁵ used STEM-ADF to investigate in details antiphase boundaries on small bilayer and on monolayer films, which are important to understand the transport properties in MoS₂ films. Ly *et al.*¹¹⁶ correlates the atomic structure of GBs with the transport properties of MoS₂ monolayers. This was achieved by measuring the transport across single grain boundaries with high-resolution TEM and first-principles calculations. The correlation of different merging angles, atomic structure, and field-effect mobility was performed. The results presented a strong relationship between the nature of the GB and the electrostatic barriers responsible for charge mobility.

The bonding characteristics between Mo and S in a MoS₂ monolayer make possible the formation of many different types of dislocation cores, which includes not only the conventional five- and seven-fold (5/7 and 6/8) rings, but also additional core with 4/4, 4/6, 4/8, and 6/8 fold rings that form different grain boundary structures. Figure 4e–i¹⁰³ depicts a grain boundary with two grains meeting each other with an angle of 18.5° . This grain

boundary is composed mainly of 5/7 and 6/8 dislocations, but 4/8 dislocations can also be observed.

van der Zande *et al.*¹¹⁷ grew grains with sizes of up to 120 μm and characterized the merging points of the MoS₂ grains with atomic resolution using STEM-ADF. They studied in detail a mirror twin boundary in a 6-pointed star MoS₂ flake. They showed that the grain boundary has a zigzag pattern exhibiting faceting of $\pm 20^\circ$. The atomic resolution investigation showed a majority of dislocations comprised 4/8 rings with a recurring ring motif periodicity of 8–4–4 as shown in Figure 4j–l.¹¹⁷ Various similar studies on grain boundary studies can also be found in the literature.^{118–124}

Garcia *et al.*¹²⁵ also investigated electron irradiation damage on MoS₂ films using an C_s aberration-corrected STEM beam at different voltages (80, 120, and 200 kV) to study the defects produced during irradiation and determined that 80 kV is the most efficient voltage to avoid damage during the imaging process. TMDs can also undergo a phase transition depending on the surrounding conditions.^{126,127} These phase transitions can be used to alter properties of the material without the addition or removal of atoms. Lin *et al.*¹²⁸ investigated the phase transition between the semiconducting (2H) and

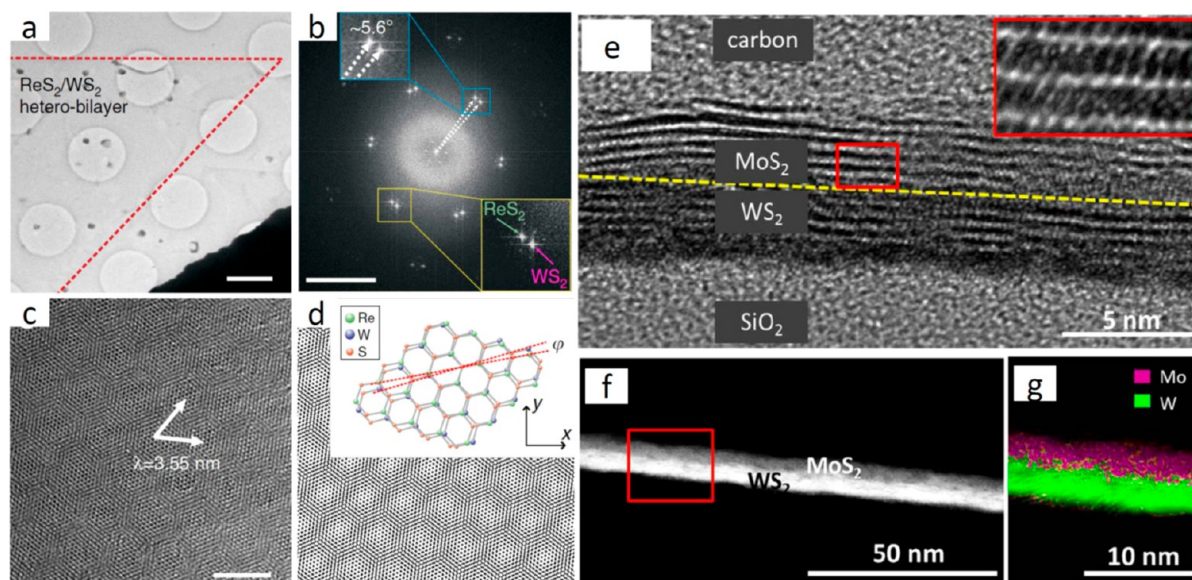


Figure 6. Structure characterization of ReS_2/WS_2 twinned vertical heterostructure. (a) Low-magnification TEM image of the ReS_2/WS_2 twinned vertical heterostructures, where a triangle crystal of ReS_2/WS_2 heterobilayer is marked. (b) Fast Fourier transform (FFT) of the heterostructure. The insets show the two patterns of ReS_2 (green) and WS_2 (purple) with a rotation angle to be about 5.6° . (c) HRTEM image of ReS_2/WS_2 twinned vertical heterostructures showing the resulting Moiré pattern. (d) Tentative orientation model of rotating the upper ReS_2 by an angle of 5.6° with respect to the ground WS_2 . Inset is the atomistic illustration of the heterostructure of ReS_2/WS_2 with their respective lattice constants and a misalignment angle ϕ . Scale bar, $1\ \mu\text{m}$ in (a); $4\ \text{nm}^{-1}$ in (b), and $4\ \text{nm}$ in (c). (e) Cross-sectional HRTEM of a vertically stacked MoS_2/WS_2 heterostructure film, revealing a nearly clean heterointerface of MoS_2/WS_2 . (f) Cross-sectional STEM-ADF image of a vertically stacked MoS_2/WS_2 heterostructure and (g) its corresponding EDX elemental mapping image. Panels (a–d) reproduced with permission from ref 132. Copyright 2016 Nature Publishing Group. Panels (e–g) reproduced with permission from ref 133. Copyright 2016 Science.

metallic (1T) phases of monolayered MoS_2 . To observe the dynamic displacement of atoms during the phase transformation, they used STEM-ADF working with an acceleration voltage of 60 kV. The phase transition was induced through heating ($400\text{--}700\ ^\circ\text{C}$) a MoS_2 specimen doped with 0.6 at% Re. As shown in Figure 5a–k, the MoS_2 film has a 2T phase, with a honeycomb structure. With time, two band-like structures gradually form along two zig-zig directions. When two of the nonparallel band-like structures come in to contact, the densely packed atoms at the corner formed are forced to move toward an area with lower atomic concentration so as to release stress and as a consequence, the 1T phase with a triangular shape forms.

TMD HETEROSTRUCTURES

TMD–TMD Heterostructures. Lateral Heterostructures.

The synthesis of different lateral heterostructure configurations has been demonstrated for graphene with other materials^{129,130} as well as for TMDs. Duan *et al.*¹³¹ synthesized and characterized different types of lateral heterostructures based on TMDs. The atomic and microstructure characterization of these heterostructures was accomplished using for the most part using high-resolution TEM and SAED along with supporting analytical techniques, such as EDX.

The SAED pattern of the $\text{MoS}_2\text{--MoSe}_2$ interface of the lateral heterostructure shows a typical hexagonal symmetry with slightly different lattice spacings ($2.70\ \text{Å}$ for the MoS_2 plane and $2.78\ \text{Å}$ for the MoSe_2 plane), which allows one to distinguish the different lateral planes. Further confirmation of the lateral heterostructure was achieved by collecting EDX linescans, which clearly showed an inverse modulation of the S and Se distribution signal. Thus, strong evidence for a

monolayered lateral heterostructures was obtained.¹³¹ A similar investigation was carried out on $\text{WS}_2\text{--WSe}_2$ lateral heterostructures. The data showed that SAED peaks appear at 2.70 and $2.81\ \text{Å}$, which correspond to WS_2 and WSe_2 lattice spacings, respectively. Again chemical modulation of the EDX signals also showed obvious differences in the regions with S and Se.¹³¹

Vertical Heterostructures. TEM characterization is also crucial to assess the structural features from vertical TMD heterostructures. Homogeneous vertical stacking of ReS_2 and WS_2 was synthesized and characterized by Zhang *et al.*¹³² The TEM characterization of the high-quality triangular heterostructures indicated that they follow a triangular form as shown in Figure 6a. The FFT of the heterostructure presented in Figure 6b shows two hexagonal patterns with a rotation angle of 5.6° with respect to each other. Furthermore, high-resolution TEM studies showed a clear Moiré pattern formed due to the tilt angle between the two layers. The Moiré pattern has a period of $3.55\ \text{nm}$ as presented Figure 6c. Image simulations of the heterostructure with a rotation of the top ReS_2 layer with respect to the bottom WS_2 layer shows a similar pattern to that obtained experimentally, thus, confirming the stacking twist of the two TMDs.

Apart from the regular high-resolution TEM and high-resolution STEM characterization, insights into the cross-section of vertical heterostructures is also necessary for a full characterization. Such investigations reveal how the TMD layers are stacked. Figure 6e–g shows a multilayer structure composed of MoS_2/WS_2 . The inset shows the atomic configuration of the interface between MoS_2 and WS_2 , confirming that these two different layers have a seamless heterointerface.¹³³

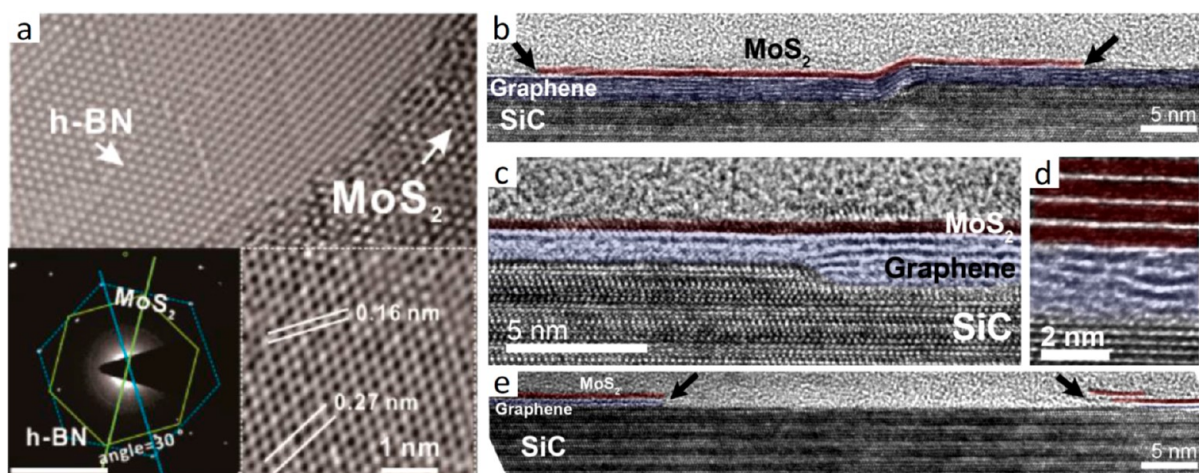


Figure 7. (a) TEM characterization of MoS₂/h-BN heterostructure. SAED patterns corresponding to the heterostructures is shown in the inset; the scale bar is 0.2 nm. The spots in the green dashed hexagons indicate the (110) plane of MoS₂, and the spots in the blue dashed hexagons indicate the (1010) plane of BN. (b) Cross-sectional HRTEM of MoS₂/Graphene demonstrating the nucleation and subsequent lateral growth of MoS₂ on a SiC step edge covered with graphene. In this case, the graphene thickness is consistent across the step, resulting in bending of the graphene and variation in strain of the graphene layer. On the other hand, when the top graphene layer remains flat as seen in (c), the MoS₂ grows without regard of the changing morphology below. When the underlying graphene is defective, additional MoS₂ adlayers are present as presented in (d), which indicates that defects in the graphene can produce MoS₂. Finally, MoS₂ nucleation and growth is promoted by the presence of graphene, whereas often it is found to be absent on bare SiC as demonstrated in (e). Panel (a) reproduced from ref 135. Copyright 2016 American Chemical Society. Panels (b–e) reproduced from ref 136. Copyright 2014 American Chemical Society

The two different layers were visualized using TEM and STEM imaging, as can be seen in Figure 6e,f. Chemical analysis, through EDX, also provide a clear difference between the two materials as shown in Figure 6g. The presence of multiple stacking alignments between the layers can be seen by the multiple rotation angles in the SAED.

TMD: OTHER 2D MATERIALS

Layered TMDs can also form heterostructures with different 2D materials.¹³⁴ Fu *et al.*¹³⁵ synthesized an MoS₂ layer on top of an h-BN layer. Similar to the TMD-TMD heterostructures, it is possible to clearly observe areas containing different layers as shown in Figure 7a. SAED was acquired for the heterostructure and it is possible to see two different hexagonal patterns with a 30° angle rotation with respect to each other. The inner spots forming the green hexagon correspond to the MoS₂ layer and the outer spots forming the larger blue hexagon correspond to the h-BN layer.

Cross-section samples of hybrid TMDs and other 2D materials also provide important interface and structural information. Lin *et al.*¹³⁶ characterized monolayers of MoS₂ and WS₂ grown atop epitaxial graphene. The clear stacking of a monolayered MoS₂ film on top of few-layer graphene is provided in Figure 7b–e. High-resolution TEM clearly demonstrates the interface of the vertical heterojunction between the MoS₂ and graphene. They also found that the presence of defects on the graphene bottom layers almost always leads to the growth of multilayered MoS₂ films, as shown in Figure 6d. Moreover, MoS₂ was observed to grow only on top of the graphene, suggesting that graphene may serve as a catalyst for its growth (Figure 6e). It is also worth mentioning at this point that TMDs have also been synthesized together with other nanostructures such as carbon nanotubes (CNTs). CNTs were shown to serve a support or as a system to encapsulate small ribbons of monolayered MoS₂ and WS₂.^{137,138}

OTHER TECHNIQUES FOR TMD CHARACTERIZATION

The focus of this review is to present the plethora of techniques and capabilities available for spatial and temporal characterization of TMD using TEM/STEM. However, the reader should be aware that other techniques can and are used to also assess structural and spectroscopic information about TMDs in their own matter. For example, in scanning electron microscopy (SEM) a focused beam of electrons interacts with the atoms of the specimen, producing different signals that provides information about the specimen topography and composition. Although with SEM atomic resolution of 2D materials has not been reported. SEM can be seen as a complementary technique to characterize 2D materials at low resolution and large areas to provide mainly morphological information on the specimen such as shape of the flakes and rough estimation of the number of layers as well as elemental mapping over large areas. Although SEM does not offer the high-resolution offered in TEM, this technique offers a quick and easy way to assess the most basic features of specimens. Xie *et al.*¹³⁹ used SEM as an easy approach to characterize the morphology of MoS₂ monolayers grown with chemical vapor deposition under different conditions. They were able to investigate the shape evolution of MoS₂ crystal growth. Lang *et al.*¹⁴⁰ used SEM imaging combined with EDX to determine the number of layers of MoS₂ and MoS₂/WSe₂. They claim that their methods is a nondestructive technique to characterize the number of layers in TMDs and 2D materials and their heterostructures in general. They used atomic force microscopy to confirm their results.

Atomic force microscopy (AFM) is a type of scanning probe microscopy (SPM) technique that can also be a powerful tool to characterize 2D materials. It mainly works using a cantilever with an atomically sharp tip that scans/rasters over the specimen. When the tip approaches the surface of the specimen, short-range attractive/repulsive forces between the

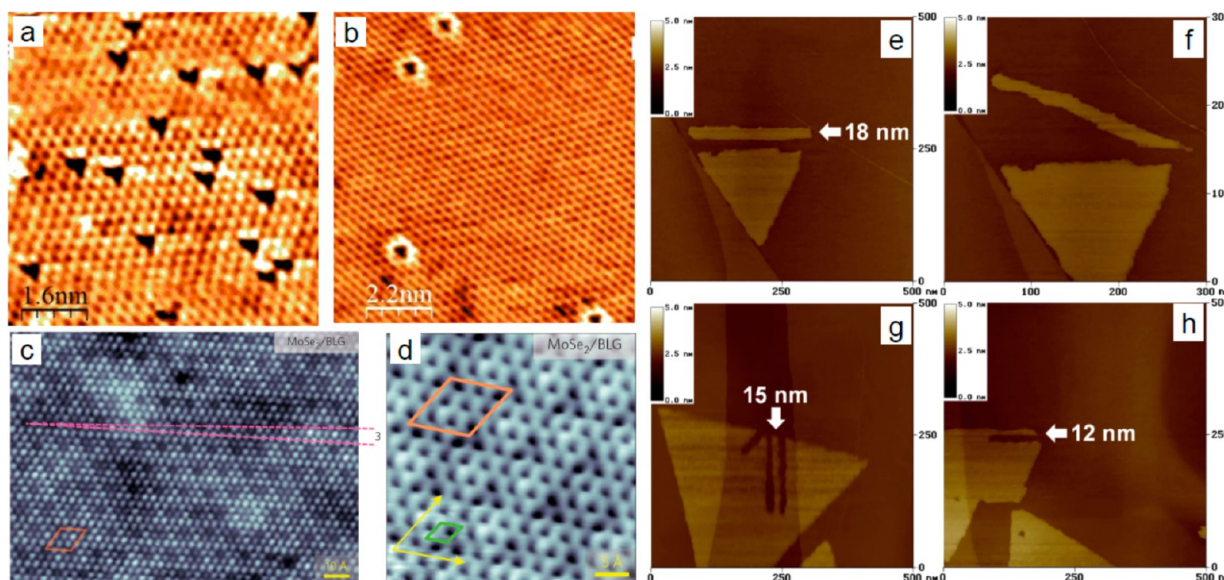


Figure 8. (a,b) Atomic resolution STM images ($V_{\text{bias}} = 50$ mV, $I_{\text{tunneling}} = 3$ nA) of single-layer MoS₂ with triangular- and circular-shaped point defects, respectively. (c) STM image of monolayer MoSe₂ showing a $9.7 \text{ \AA} \times 9.7 \text{ \AA}$ Moiré pattern with an angle of 3° between the Moiré pattern and the MoSe₂ lattice ($V_{\text{bias}} = -0.9$ V, $I_{\text{tunneling}} = 3$ pA, $T = 5$ K). (d) High-resolution STM image of MoSe₂ ($V_{\text{bias}} = -1.53$ V, $I_{\text{tunneling}} = 3$ nA, $T = 5$ K). (e–h) MoS₂ nanoribbons cut by STM nanolithography on highly ordered graphite: (e) ~ 18 nm wide MoS₂ ribbon, (f) same nanoribbon moved by the STM tip, (g) ~ 15 nm, and (h) ~ 12 nm wide MoS₂ ribbons. Panels (a,b) reproduced with permission from ref 146. Copyright 2016 Science. Panels (c,d) reproduced with permission from ref 147. Copyright 2014 Nature Publishing Group. Panels (e–h) reproduced with permission from ref 149. Copyright 2016 Elsevier.

surface and the tip causes the cantilever to deflect. A position-sensitive photodiode can detect these deflections and it is possible to create an image of the specimen topography. This simple working mode can reveal detailed topographic information such as number of layers¹⁴¹ and contaminants on the surface. It is however known that contaminants can cause measurement discrepancies. Therefore, prior to AFM measurement it is useful to use methods for cleaning the surface such as with annealing. Similar disturbances from contaminants can also influence measurements in TEM, especially due to residual contaminants from transfer methods as presented before. Strategies to overcome contaminants is beneficial to both TEM and AFM measurements. Recently, Godin *et al.*¹⁴² presented a model to remove water from WS₂ samples reducing discrepancies in height measurements of the layers. To overcome this problem they used high-vacuum annealing, which remove the contaminants from the WS₂ surface and produced AFM images with high set point and low amplitudes. This avoided contrast inversions during the measuring and the correct topography can be investigated. Ly *et al.*¹⁴³ reported the use of AFM to study the edge effect on the formation of wrinkles and buckles in single atomic layers of WS₂ crystals. Their study suggest that the observation of domain contrast and edge enhancement may be caused by buckling processes associated with edges of the WS₂ flakes instead of by intrinsic defects. This result can also be generalized to all 2D materials, but as atomic resolution in this case is not achieved with AFM, TEM plays an important complementary role to proof or disprove the existence of intrinsic defects with images in atomic scale. AFM can also work in different modes, which allow probing specific properties of 2D materials, such as mechanical, electro-mechanics, spectroscopic and electrochemical properties.¹⁴⁴ For example, Choi *et al.*¹⁴⁵ investigated how commonly used solvents significantly changes the physical properties of MoS₂

and WSe₂ monolayers. For this, they used conductive AFM before and after immersion of the above-mentioned monolayers in solvents such as chloroform, toluene, acetone and 2-propanol. The immersion of the TMD monolayers in these solvents caused changes in the carrier density and highlights the importance of careful characterization and handling of TMD prior to use in any application. The authors also claim that the sensitivity of MoS₂ and WSe₂ to the solvents raises the viability of these monolayers to be used in chemical sensors. Such electric properties can also be assessed in TEM, however with AFM such measurements can be easily achieved in different atmospheric conditions and large areas of the TMD monolayer.

Scanning tunneling microscopy (STM) is another powerful SPM technique to investigate 2D materials. It also uses an atomically sharp conducting tip that scans the specimen. When the conducting tip is very near to the surface, a bias voltage is applied that can allow the electrons to tunnel through the vacuum between the surface and the tip. This tunneling current is dependent on the position of the tip, applied bias voltage and local density of states of the specimen. This technique allows atomic resolution imaging, probing of the local electronic states of the sample and even atomic nanomanipulations. However, it requires exceptionally clean and stable surfaces, high-quality tips, state of the art electronics and high-performance vibration protections. Although STM may provide a high spatial resolution, it is very challenging to obtain dynamic information on specimen as single measurements may take very long and the reduced size of scanning areas. For example, Vancsó *et al.*¹⁴⁶ reported the characterization of point defects on MoS₂ monolayers using STM. They were able to achieve high-resolution images of intrinsic triangular and circular defects on MoS₂ monolayers as shown in Figure 8a,b. Apart from the enormous challenge to image such defect areas with STM, it provides the advantage of

studying such vacancies without the influence of local electron-beam-induced damage. Ugeda *et al.*¹⁴⁷ used the spectroscopic capabilities of STM to investigate the electronic properties of layered MoSe₂ grown on epitaxial graphene bilayers, as shown in Figure 8c,d, by determining the band gap of this heterostructure. Similar band gap experiments were also carried out by Hill *et al.*¹⁴⁸ on MoS₂/WS₂ heterostructures. Here again, it is useful to mention that EELS measurements inside a TEM column would also be a possible alternative to determine the band gap of these heterostructures. This can be achieved in the TEM by filtering the incident electron beam to a fraction of the energy distribution in order to at the same time reduce the intensity of the beam and increase the energy resolution of the spectrum. However, in the TEM it is impossible to avoid completely electron-induced damage or influences in the measurement. The nanomanipulation of TMDs can also be achieved by STM, which can be used for nanoengineering nanoelectronic devices. Koós *et al.*¹⁴⁹ used STM lithography to cut monolayered MoS₂ films grown on highly ordered graphite. They were able to create MoS₂ nanoribbons from 18 nm down to 12 nm with precision edge roughness, as shown in Figure 8e–h. The cutting could be achieved in any crystallographic orientation. Additionally, they were also able to move these nanoribbons in any direction or rotation on the graphite. Such manipulation capabilities suggest the possibility to assemble intricate nanocircuits and complex devices. Using a highly focused electron beam it is also possible to achieve state-of-the-art possibilities in nanoengineering and nanomanipulation. However, the displacement of pieces of the specimen remains a disadvantage of TEM over STM in this respect.

FUTURE OUTLOOK

The rise of TMDs is phenomenal and is in many ways par with that of graphene. This is also reflected in important works from transmission electron microscopy of such materials. Indeed, recent investigations demonstrate a great and rising interest in the use of TEM to unravel the structural and dynamic aspects (Figure 9a) of TMDs under electron beam irradiation using aberration-corrected TEM and STEM as well as analytical methods performed inside the TEM column such as EELS and EDX. Although the synthesis methods of TMDs have improved, rendering monolayers with larger areas and less defects, the synthesis process is still difficult to control and the generation of intrinsic defects is to date is an unavoidable reality.^{108,150} These imperfections strongly regulate many of the physical and chemical properties of TMDs. The biggest interest lies in the control of the materials functionality, which can be achieved, for example by doping or atom substitution¹⁵¹ as shown in Figure 9b. This doping can happen through impurities during synthesis,¹⁵² absorption of metals^{153,154} or functionalization with molecules.^{150,155–157}

The broad range of properties offered by TMDs especially their potential for tuned properties make them exciting and relevant materials in the current 2D layered materials age. Indeed, our ability to stack 2D layers at will to design heterostructures, in essence, allows us to create truly artificial materials with truly controllable properties. This undoubtedly provides a momentous technological opportunity which will impact mankind's future in a positive manner in unimaginable ways. For example, the use of TMDs and their heterostructures to build field-effect transistors^{158–160} as shown in Figure 9d and other devices.^{161–166} Critical to the development of TMD

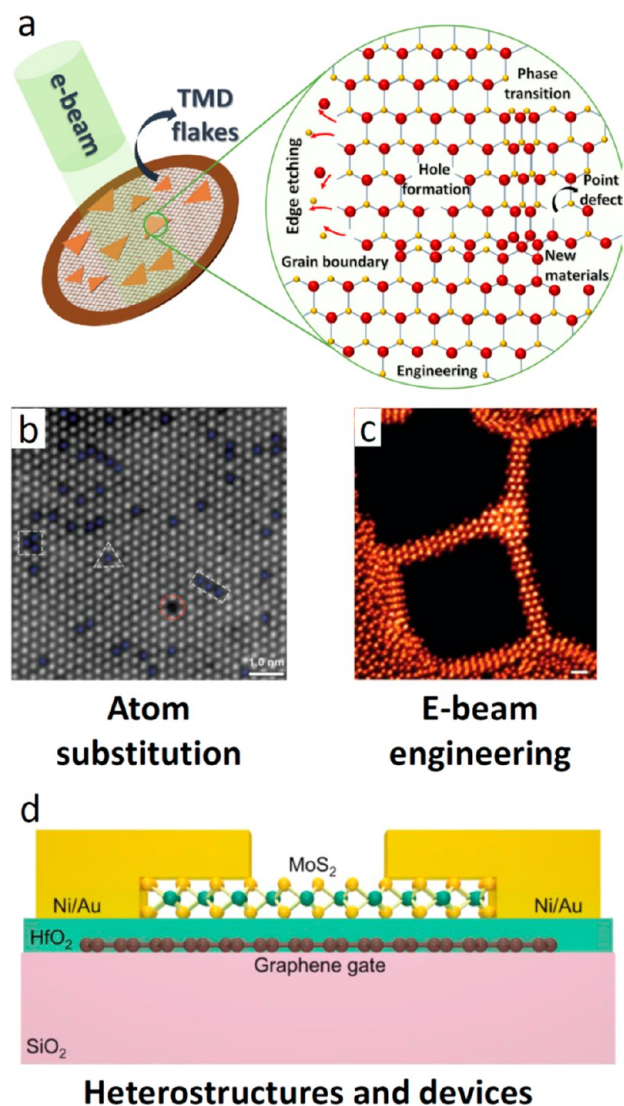


Figure 9. (a) TMD flakes suspended in vacuum can be studied under electron beam irradiation leading to a plethora of dynamic phenomena such as hole formation, phase transformation, edge etching and atomic dislocation. These phenomena can be used for controllable electron-beam-driven engineering and creation of different materials. (b) Structural reconstruction of a WS₂ monolayer indicating the distribution of Nb dopants (blue, Nb sites; white, W sites; black holes, metal vacancies). Reproduced with permission from ref 151. Copyright 2016 Wiley. (c) Fabrication of nanowires from TMD monolayers using a focused electron beam. The image shows a ramified Y junction made of three MoSe nanowires. Reproduced with permission from ref 82. Copyright 2014 Nature Publishing Group. (d) Schematic of the graphene bottom local-gate MoS₂ field-effect transistor. Reproduced from ref 158. Copyright 2018 American Chemical Society.

materials is the use of electron microscopy which allows us to understand the structure, structure–property relationships, engineering and chemistry of these materials at the atomic level.

In this review we also dedicated a section to present other techniques that are used to characterize TMDs, among which are SEM, AFM and STM. Each one of these highly advanced tools present its individual advantages and disadvantages. For example, SEM provides a way to quickly assess the morphology and chemical composition of large areas. AFM allows the

probing of the surface of TMDs with high accuracy. Due to the many different AFM modes, it is possible to probe additional properties such as mechanical and electrical ones. However, SEM and AFM lack in the capabilities to study in detailed local properties at the atomic scale of TMD lattices. Such drawback can be overcome using STM, which offers the possibilities of nanomanipulations as well as both structural and analytical investigation of TMDs. Although such STM measurements can reach comparable resolution to the ones obtained in TEM, STM high-quality measurements are extremely challenging and long to perform. This requirement makes STM lacks almost completely in temporal resolution, which can be performed in TEM with atomic resolution in the most advanced cameras already available in the market. Therefore, as a whole, *in situ* TEM offers not only ultimate spatial and temporal resolution, but also additional state-of-the-art spectroscopic capabilities and nanomanipulation. No other technique unites all these possibilities in a single equipment at such a superior atomic scale resolution.

Electron microscopy offers an important tool to easily reach atomic characterization of materials, however the controllable electron-driven engineering and tuning of properties of TMDs and other 2D materials remain a great challenge.^{84,167–169} The controllable engineering of TMDs is essential to directly control electrical, optical, magnetic and catalytic properties.⁸⁴ This challenge starts with the understanding of the most fundamental mechanisms of interaction between the atoms and the electron beam.^{170–172} For example, the idea to intentionally drill nanopores in MoS₂ monolayers¹⁷³ and nanowires¹⁷⁴ or nanojunctions (Figure 9c). The results discussed in this review points out to a rather challenging, but feasible plan to intentionally move single atoms and defects across the lattice of materials using an electron beam just like it has been already achieved with scanning probe microscopy techniques. If the current progress in engineering TMD monolayers and other 2D materials is anything to go by, then the future of TEM and TMDs is indeed very exciting.

Although a lot has been achieved over the past few years in the understanding of the *in situ* growth of different 2D materials^{175,176} as well as the unravelling of the crystalline structure of TMDs and TMD heterostructures there remains plenty to learn still with respect to the dynamic mechanisms involved in their *in situ* synthesis and electron beam interactions.¹⁷⁷ In the future we anticipate more systematic studies dedicated to investigate mainly the *in situ* growth of TMDs and to better comprehend the influence of TEM acceleration voltage on 2D TMDs.

To finalize, we also envision a future where the scalability of electron-beam-engineered circuits and nanodevices can be achieved. For this, highly advanced assembly lines with specific functions containing electron beam sources could perform the desired tasks. However, this futuristic approach could only be achieved with the use of highly advanced artificial intelligent softwares, which when linked to the electron beam machinery could recognize with atomic precision the areas that need to be modified and designed as the final application requires. In this manner, we could not only reach scalability of electron beam engineering, but also automation of the process. TEM and its techniques provide a complete and powerful window to understand the structural, dynamic and chemical properties of TMDs (and other 2D materials) at the atomic scale, which are necessary for any further implementation of TMDs in future nanodevices.

AUTHOR INFORMATION

Corresponding Author

*E-mail: mhr1967@yahoo.com.

ORCID

Jinbo Pang: 0000-0001-6965-4166

Lei Fu: 0000-0003-1356-4422

Zhongfan Liu: 0000-0003-0065-7988

Mark H. Rummeli: 0000-0002-4448-1569

Notes

The authors declare no competing financial interest.

ACKNOWLEDGMENTS

M.H.R. and L.F. thank the Chinesisch-Deutsche Zentrum für Wissenschaftsförderung (project GZ 1400). The following are also gratefully acknowledged. The National Natural Science Foundation of China (No. 51672181), the National Science Center (Poland) for the financial support within the frame of the Sonata Program (No. 2014/13/D/STS/02853), and the Opus program (No. 2015/19/B/STS/03399).

VOCABULARY

2D materials, class of crystalline nanomaterials that can be formed by a single atom layer; heterostructures combination of multiple in- and out-of-plane 2D materials used to design innovative artificial materials with precise properties tuned for specific applications; **electron knock-on damage**, atomic displacements in the crystalline lattice of materials caused by elastic scattering during electron irradiation; **radiolysis**, referred to a damaging process as the result of inelastic scattering between incident electron with the specimen leading to degradation of crystalline lattice; **electron beam engineering**, nanomanipulation of materials with atomic precision using an electron beam in order to investigate and tailor materials properties

REFERENCES

- (1) Dickinson, R. G.; Pauling, L. The Crystal Structure of Molybdenite. *J. Am. Chem. Soc.* **1923**, *45*, 1466–1471.
- (2) An, S.; Kim, Y. H.; Lee, C.; Park, D. Y.; Jeong, M. S. Exfoliation of Transition Metal Dichalcogenides by a High-Power Femtosecond Laser. *Sci. Rep.* **2018**, *8*, 12957.
- (3) Peng, J.; Wu, J.; Li, X.; Zhou, Y.; Yu, Z.; Guo, Y.; Wu, J.; Lin, Y.; Li, Z.; Wu, X.; Wu, C.; Xie, Y. Very Large-Sized Transition Metal Dichalcogenides Monolayers from Fast Exfoliation by Manual Shaking. *J. Am. Chem. Soc.* **2017**, *139*, 9019–9025.
- (4) Li, H.; Wu, J.; Yin, Z.; Zhang, H. Preparation and Applications of Mechanically Exfoliated Single-Layer and Multilayer MoS₂ and WSe₂ Nanosheets. *Acc. Chem. Res.* **2014**, *47*, 1067–1075.
- (5) Jawaid, A.; Che, J.; Drummy, L. F.; Bultman, J.; Waite, A.; Hsiao, M.; Vaia, R. A. Redox Exfoliation of Layered Transition Metal Dichalcogenides. *ACS Nano* **2017**, *11*, 635–646.
- (6) Budania, P.; Baine, P. T.; Montgomery, J. H.; McNeill, D. W.; Neil Mitchell, S. J.; Modreanu, M.; Hurley, P. K. Comparison Between Scotch Tape and Gel-Assisted Mechanical Exfoliation Techniques for Preparation of 2D Transition of 2D Transition Metal Dichalcogenide Flakes. *Micro Nano Lett.* **2017**, *12*, 970–973.
- (7) Joensen, P.; Frindt, R. F.; Morrison, S. R. Single-Layer MoS₂. *Mater. Res. Bull.* **1986**, *21*, 457–461.
- (8) Novoselov, K. S.; Geim, A. K.; Morozov, S. V.; Jiang, D.; Zhang, Y.; Dubonos, S. V.; Grigorieva, I. V.; Firsov, A. A.; Novoselov, K. S. Electric Field Effect in Atomically Thin Carbon Films. *Science* **2004**, *306*, 666–669.

- (9) Andriotis, A. N.; Richter, E.; Menon, M. Prediction of a New Graphenelike Si_2BN Solid. *Phys. Rev. B: Condens. Matter Mater. Phys.* **2016**, *93*, 081413.
- (10) Warner, J. H.; Rummeli, M. H.; Bachmatiuk, A.; Büchner, B. Atomic Resolution Imaging and Topography of Boron Nitride Sheets Produced by Chemical Exfoliation. *ACS Nano* **2010**, *4*, 1299–1304.
- (11) Pang, J.; Bachmatiuk, A.; Yin, Y.; Trzebicka, B.; Zhao, L.; Fu, L.; Mendes, R. G.; Gemming, T.; Liu, Z.; Rummeli, M. H. Applications of Phosphorene and Black Phosphorus in Energy Conversion and Storage Devices. *Adv. Energy Mater.* **2018**, *8*, 1702093.
- (12) Anasori, B.; Lukatskaya, M. R.; Gogotsi, Y. 2D Metal Carbides and Nitrides (MXenes) for Energy Storage. *Nat. Rev. Mater.* **2017**, *2*, 16098.
- (13) Naguib, M.; Mochalin, V. N.; Barsoum, M. W.; Gogotsi, Y. 25th Anniversary Article: MXenes: A New Family of Two-Dimensional Materials. *Adv. Mater.* **2014**, *26*, 992–1005.
- (14) Hong Ng, V. M.; Huang, H.; Zhou, K.; Lee, P. S.; Que, W.; Xu, J. Z.; Kong, L. B. Recent Progress in Layered Transition Metal Carbides and/or Nitrides (MXenes) and Their Composites: Synthesis and Applications. *J. Mater. Chem. A* **2017**, *5*, 3039–3068.
- (15) Bampoulis, P.; Zhang, L.; Safaei, A.; van Gastel, R.; Poelsema, B.; Zandvliet, H. J. W. Germanene Termination of Ge_2Pt Crystals on Ge(110). *J. Phys.: Condens. Matter* **2014**, *26*, 442001.
- (16) Reis, F.; Li, G.; Dudy, L.; Bauernfeind, M.; Glass, S.; Hanke, W.; Thomale, R.; Schäfer, J.; Claessen, R. Bismuthene on a SiC Substrate: A Candidate for a High-Temperature Quantum Spin Hall Material. *Science* **2017**, *357*, 287–290.
- (17) Zhao, J.; Liu, H.; Yu, Z.; Quhe, R.; Zhou, S.; Wang, Y.; Liu, C. C.; Zhong, H.; Han, N.; Lu, J.; Yao, Y.; Wu, K. Rise of Silicene: A Competitive 2D Material. *Prog. Mater. Sci.* **2016**, *83*, 24–151.
- (18) Khandelwal, A.; Mani, K.; Karigerasi, M. H.; Lahiri, I. Phosphorene - The Two-Dimensional Black Phosphorous: Properties, Synthesis and Application. *Mater. Sci. Eng., B* **2017**, *221*, 17–34.
- (19) Fadaie, M.; Shahtahmassebi, N.; Roknabad, M. R.; Gulseren, O. Investigation of New Two-Dimensional Materials Derived from Stanene. *Comput. Mater. Sci.* **2017**, *137*, 208–214.
- (20) Gong, C.; Zhang, Y.; Chen, W.; Chu, J.; Lei, T.; Pu, J.; Dai, L.; Wu, C.; Cheng, Y.; Zhai, T.; Li, L.; Xiong, J. Electronic and Optoelectronic Applications Based on 2D Novel Anisotropic Transition Metal Dichalcogenides. *Adv. Sci.* **2017**, *4*, 1700231.
- (21) Ahmed, S.; Yi, J. Two-Dimensional Transition Metal Dichalcogenides and Their Charge Carrier Mobilities in Field-Effect Transistors. *Nano-Micro Lett.* **2017**, *9*, 50.
- (22) Zhou, J.; Qin, J.; Guo, L.; Zhao, N.; Shi, C.; Liu, E.; He, F.; Ma, L.; Li, J.; He, C. Scalable Synthesis of High-Quality Transition Metal Dichalcogenide Nanosheets and Their Application as Sodium-Ion Battery Anodes. *J. Mater. Chem. A* **2016**, *4*, 17370–17380.
- (23) Yang, E.; Ji, H.; Jung, Y. Two-Dimensional Transition Metal Dichalcogenide Monolayers as Promising Sodium Ion Battery Anodes. *J. Phys. Chem. C* **2015**, *119*, 26374–26380.
- (24) Wu, S.; Du, Y.; Sun, S. Transition Metal Dichalcogenide Based Nanomaterials for Rechargeable Batteries. *Chem. Eng. J.* **2017**, *307*, 189–207.
- (25) Akama, T.; Okita, W.; Nagai, R.; Li, C.; Kaneko, T.; Kato, T. Schottky Solar Cell Using Few-Layered Transition Metal Dichalcogenides Toward Large-Scale Fabrication of Semitransparent and Flexible Power Generator. *Sci. Rep.* **2017**, *7*, 11967.
- (26) Thilagam, A. Transition-Metal Dichalcogenide Heterostructure Solar Cells: A Numerical Study. *J. Math. Chem.* **2017**, *55*, 50–64.
- (27) Hu, Y.; Huang, Y.; Tan, C.; Zhang, X.; Lu, Q.; Sindoro, M.; Huang, X.; Huang, W.; Wang, L.; Zhang, H. Two-Dimensional Transition Metal Dichalcogenide Nanomaterials for Biosensing Applications. *Mater. Chem. Front.* **2017**, *1*, 24–36.
- (28) Zappa, D. Molybdenum Dichalcogenides for Environmental Chemical Sensing. *Materials* **2017**, *10*, 1418.
- (29) Feierabend, M.; Berghäuser, G.; Knorr, A.; Malic, E. Proposal for Dark Exciton Based Chemical Sensors. *Nat. Commun.* **2017**, *8*, 14776.
- (30) Ping, J.; Fan, Z.; Sindoro, M.; Ying, Y.; Zhang, H. Recent Advances in Sensing Applications of Two-Dimensional Transition Metal Dichalcogenide Nanosheets and Their Composites. *Adv. Funct. Mater.* **2017**, *27*, 1605817.
- (31) Lee, E.; Yoon, Y. S.; Kim, D. J. Two-Dimensional Transition Metal Dichalcogenides and Metal Oxide Hybrids for Gas Sensing. *ACS Sens.* **2018**, *3*, 2045–2060.
- (32) Chimene, D.; Alge, D. L.; Gaharwar, A. K. Two-Dimensional Nanomaterials for Biomedical Applications: Emerging Trends and Future Prospects. *Adv. Mater.* **2015**, *27*, 7261–7284.
- (33) Kalantar-zadeh, K.; Ou, J. Z.; Daeneke, T.; Strano, M. S.; Pumera, M.; Gras, S. L. Two-Dimensional Transition Metal Dichalcogenides in Biosystems. *Adv. Funct. Mater.* **2015**, *25*, 5086–5099.
- (34) Li, X.; Shan, J.; Zhang, W.; Su, S.; Yuwen, L.; Wang, L. Recent Advances in Synthesis and Biomedical Applications of Two-Dimensional Transition Metal Dichalcogenide Nanosheets. *Small* **2017**, *13*, 1602660.
- (35) Kolobov, A. V.; Tominaga, J. *Two-Dimensional Transition-Metal Dichalcogenides*; Springer International Publishing: Switzerland, 2016.
- (36) Wang, Y.; Li, L.; Yao, W.; Song, S.; Sun, J. T.; Pan, J.; Ren, X.; Li, C.; Okunishi, E.; Wang, Y. Q.; Wang, E.; Shao, Y.; Zhang, Y. Y.; Yang, H.; Schwier, E. F.; Iwasawa, H.; Shimada, K.; Taniguchi, M.; Cheng, Z.; Zhou, S.; et al. *et al.* Monolayer PtSe_2 , a New Semiconducting Transition-Metal-Dichalcogenide, Epitaxially Grown by Direct Selenization of Pt. *Nano Lett.* **2015**, *15*, 4013–4018.
- (37) Guzman, D. M.; Strachan, A. Role of Strain on Electronic and Mechanical Response of Semiconducting Transition-Metal Dichalcogenide Monolayers: An *Ab-Initio* Study. *J. Appl. Phys.* **2014**, *115*, 243701.
- (38) Nayeri, M.; Moradinasab, M.; Fathipour, M. The Transport and Optical Sensing Properties of MoS_2 , MoSe_2 , WS_2 and WSe_2 Semiconducting Transition Metal Dichalcogenides. *Semicond. Sci. Technol.* **2018**, *33*, 025002.
- (39) Lee, J.; Huang, J.; Sumpter, B. G.; Yoon, M. Strain-Engineered Optoelectronic Properties of 2D Transition Metal Dichalcogenide Lateral Heterostructures. *2D Mater.* **2017**, *4*, 021016.
- (40) Zhang, H.; Ji, J.; Gonzalez, A. A.; Choi, J. H. Tailoring Photoelectrochemical Properties of Semiconducting Transition Metal Dichalcogenide Nanolayers with Porphyrin Functionalization. *J. Mater. Chem. C* **2017**, *5*, 11233–11238.
- (41) Wang, J.; Verzhbitskiy, I.; Eda, G. Electroluminescent Devices Based on 2D Semiconducting Transition Metal Dichalcogenides. *Adv. Mater.* **2018**, *30*, 1802687.
- (42) Yu, X.; Sivula, K. Layered 2D Semiconducting Transition Metal Dichalcogenides for Solar Energy Conversion. *Curr. Opin. Electrochem.* **2017**, *2*, 97–103.
- (43) Campbell, D. J.; Eckberg, C.; Zavalij, P. Y.; Paglione, J. Intrinsic Insulating Ground State in Transition Metal Dichalcogenide TiSe_2 . *arXiv:1809.09467*, **2018**.
- (44) Lee, C. H.; Silva, E. C.; Calderin, L.; Nguyen, M. A. T.; Hollander, M. J.; Bersch, B.; Mallouk, T. E.; Robinson, J. A. Tungsten Ditetelluride: A Layered Semimetal. *Sci. Rep.* **2015**, *5*, 10013.
- (45) Zhao, S.; Hotta, T.; Koretsune, T.; Watanabe, K.; Taniguchi, T.; Sugawara, K.; Takahashi, T.; Shinohara, H.; Kitaura, R. Two-Dimensional Metallic NbS_2 : Growth, Optical Identification and Transport Properties. *2D Mater.* **2016**, *3*, 025027.
- (46) Cudazzo, P.; Müller, E.; Habenicht, C.; Gatti, M.; Berger, H.; Knupfer, M.; Rubio, A.; Huotari, S. Negative Plasmon Dispersion in 2H-NbS_2 Beyond the Charge-Density-Wave Interpretation. *New J. Phys.* **2016**, *18*, 103050.
- (47) Duvjir, G.; Choi, B. K.; Jang, I.; Ulstrup, S.; Kang, S.; Thi Ly, T.; Kim, S.; Choi, Y. H.; Jozwiak, C.; Bostwick, A.; Rotenberg, E.; Park, J. G.; Sankar, R.; Kim, K. S.; Kim, J.; Chang, Y. J. Emergence of a Metal-Insulator Transition and High-Temperature Charge-Density Waves in VSe_2 at the Monolayer Limit. *Nano Lett.* **2018**, *18*, 5432–5438.

- (48) Aras, M.; Kilic, C.; Ciraci, S. Lateral and Vertical Heterostructures of Transition Metal Dichalcogenides. *J. Phys. Chem. C* **2018**, *122*, 1547–1555.
- (49) Amin, B.; Singh, N.; Schwingenschlogl, U. Heterostructures of Transition Metal Dichalcogenides. *Phys. Rev. B: Condens. Matter Mater. Phys.* **2015**, *92*, 075439.
- (50) Qi, H.; Wang, L.; Sun, J.; Long, Y.; Hu, P.; Liu, F.; He, X. Production Methods of Van Der Waals Heterostructures Based on Transition Metal Dichalcogenides. *Crystals* **2018**, *8*, 35.
- (51) Liu, P.; Xiang, B. 2D Hetero-Structures Based on Transition Metal Dichalcogenides: Fabrication, Properties and Applications. *Sci. Bull.* **2017**, *62*, 1148–1161.
- (52) Naylor, C. H.; Parkin, W. M.; Gao, Z.; Berry, J.; Zhou, S.; Zhang, Q.; McClimon, J. B.; Tan, L. Z.; Kehayias, C. E.; Zhao, M.; Gona, R. S.; Carpick, R. W.; Rappe, A. M.; Srolovitz, D. J.; Drndic, M.; Johnson, A. T. C. Synthesis and Physical Properties of Phase-Engineered Transition Metal Dichalcogenide Monolayer Heterostructures. *ACS Nano* **2017**, *11*, 8619–8627.
- (53) Wang, S.; Tian, H.; Ren, C.; Yu, J.; Sun, M. Electronic and Optical Properties of Heterostructures Based on Transition Metal Dichalcogenides and Graphene-like Zinc Oxide. *Sci. Rep.* **2018**, *8*, 12009.
- (54) Tan, C.; Cao, X.; Wu, X.; He, Q.; Yang, J.; Zhang, X.; Chen, J.; Zhao, W.; Han, S.; Nam, G.; Sindoro, M.; Zhang, H. Recent Advances in Ultrathin Two-Dimensional Nanomaterials. *Chem. Rev.* **2017**, *117*, 6225–6331.
- (55) Liu, X.; Zhang, Z.; Wang, L.; Yakobson, B. I.; Hersam, M. C. Intermixing and Periodic Self-Assembly of Borophene Line Defects. *Nat. Mater.* **2018**, *17*, 783–788.
- (56) Zhao, X.; Kotakoski, J.; Meyer, J. C.; Sutter, E.; Sutter, P.; Krasheninnikov, A. V.; Kaiser, U.; Zhou, W. Engineering and Modifying Two-Dimensional Materials by Electron Beams. *MRS Bull.* **2017**, *42*, 667–676.
- (57) Elibol, K.; Susi, T.; Argentero, G.; Reza Ahmadpour Monazam, M.; Pennycook, T. J.; Meyer, J. C.; Kotakoski, J. Atomic Structure of Intrinsic and Electron-Irradiation-Induced Defects in MoTe₂. *Chem. Mater.* **2018**, *30*, 1230–1238.
- (58) Komsa, H.; Krasheninnikov, A. V. Engineering the Electronic Properties of Two-Dimensional Transition Metal Dichalcogenides by Introducing Mirror Twin Boundaries. *Adv. Electron. Mater.* **2017**, *3*, 1600468.
- (59) Kalinin, S. V.; Pennycook, S. J. Single-Atom Fabrication with Electron and Ion Beams: From Surfaces and Two-Dimensional Materials Toward Three-Dimensional Atom-by-Atom Assembly. *MRS Bull.* **2017**, *42*, 637–643.
- (60) Luo, C.; Wang, C.; Wu, X.; Zhang, J.; Chu, J. *In Situ* Transmission Electron Microscopy Characterization and Manipulation of Two-Dimensional Layered Materials beyond Graphene. *Small* **2017**, *13*, 1604259.
- (61) Ngoc My Duong, H.; Nguyen, M. A. P.; Kianinia, M.; Ohshima, T.; Abe, H.; Watanabe, K.; Taniguchi, T.; Edgar, J. H.; Aharonovich, I.; Toth, M. Effects of High-Energy Electron Irradiation on Quantum Emitters in Hexagonal Boron Nitride. *ACS Appl. Mater. Interfaces* **2018**, *10*, 124886.
- (62) Susi, T.; Meyer, J. C.; Kotakoski, J. Manipulating Low-Dimensional Materials Down to the Level of Single Atoms with Electron Irradiation. *Ultramicroscopy* **2017**, *180*, 163–172.
- (63) Taha, D.; Mkhonta, S. K.; Elder, K. R.; Huang, Z. Grain Boundary Structures and Collective Dynamics of Inversion Domains in Binary Two-Dimensional Materials. *Phys. Rev. Lett.* **2017**, *118*, 255501.
- (64) Winter, A.; George, A.; Neumann, C.; Tang, Z.; Mohn, M. J.; Biskupek, J.; Masurkar, N.; Reddy, A. L. M.; Weimann, T.; Hübner, U.; Kaiser, U.; Turchanin, A. Lateral Heterostructures of Two-Dimensional Materials by Electron-Beam Induced Stitching. *Carbon* **2018**, *128*, 106–116.
- (65) Rümmele, M. H.; Ta, H. Q.; Mendes, R. G.; Gonzalez-Martinez, I. G.; Zhao, L.; Gao, J.; Fu, L.; Gemming, T.; Bachmatiuk, A.; Liu, Z. New Frontiers in Electron Beam-Driven Chemistry in and Around Graphene. *Adv. Mater.* **2018**, *30*, 1800715.
- (66) Williams, D. B.; Carter, C. B. *Transmission Electron Microscopy*, 1st ed.; Springer: New York, 2009.
- (67) Egerton, R. F.; Li, P.; Malac, M. Radiation Damage in the TEM and SEM. *Micron* **2004**, *35*, 399–409.
- (68) Gu, H.; Li, G.; Liu, C.; Yuan, F.; Han, F.; Zhang, L.; Wu, S. Considerable Knock-On Displacement of Metal Atoms Under a Low Energy Electron Beam. *Sci. Rep.* **2017**, *7*, 184.
- (69) Kotakoski, J.; Jin, C. H.; Lehtinen, O.; Suenaga, K.; Krasheninnikov, A. V. Electron Knock-On Damage in Hexagonal Boron Nitride Monolayers. *Phys. Rev. B: Condens. Matter Mater. Phys.* **2010**, *82*, 113404.
- (70) Leijten, Z. J. W. A.; Keizer, A. D. A.; de With, G.; Friedrich, H. Quantitative Analysis of Electron Beam Damage in Organic Thin Films. *J. Phys. Chem. C* **2017**, *121*, 10552–10561.
- (71) Azcarate, J. C.; Fonticelli, M. H.; Zelaya, E. Radiation Damage Mechanisms of Monolayer-Protected Nanoparticles via TEM Analysis. *J. Phys. Chem. C* **2017**, *121*, 26108–26116.
- (72) Ugurlu, O.; Haus, J.; Gunawan, A. A.; Thomas, M. G.; Maheshwari, S.; Tsapatsis, M.; Mkhoyan, K. A. Radiolysis to Knock-On Damage Transition in Zeolites Under Electron Beam Irradiation. *Phys. Rev. B: Condens. Matter Mater. Phys.* **2011**, *83*, 113408.
- (73) Zhang, D.; Zhu, Y.; Liu, L.; Ying, X.; Hsiung, C.; Sougrat, R.; Li, K.; Han, Y. Atomic-Resolution Transmission Electron Microscopy of Electron Beam-Sensitive Crystalline Materials. *Science* **2018**, *359*, 675–679.
- (74) Liu, X.; Xu, T.; Wu, X.; Zhang, Z.; Yu, J.; Qiu, H.; Hong, J.-H.; Jin, C.-H.; Li, J.-X.; Wang, X.-R.; Sun, L.-T.; Guo, W. Top-down Fabrication of Sub-Nanometre Semiconducting Nanoribbons Derived from Molybdenum Disulfide Sheets. *Nat. Commun.* **2013**, *4*, 1776.
- (75) Gorantla, S.; Bachmatiuk, A.; Hwang, J.; Alsaman, H. A.; Kwak, J. Y.; Seyller, T.; Eckert, J.; Spencer, M. G.; Rümmele, M. H. A Universal Transfer Route for Graphene. *Nanoscale* **2014**, *6*, 889–896.
- (76) Mlack, J. T.; Masih Das, P.; Danda, G.; Chou, Y.-C.; Naylor, C. H.; Lin, Z.; López, N. P.; Zhang, T.; Terrones, M.; Johnson, A. T. C.; Drndic, M. Transfer of Monolayer TMD WS₂ and Raman Study of Substrate Effects. *Sci. Rep.* **2017**, *7*, 43037.
- (77) Ma, D.; Shi, J.; Ji, Q.; Zhang, Y.; Liu, M.; Feng, Q.; Song, X.; Zhang, J.; Zhang, Y.; Liu, Z. Etching-Free Transfer of Wafer-Scale MoS₂ Films. *arXiv:1501.00786*, **2015**.
- (78) Dumcenco, D. O.; Kobayashi, H.; Liu, Z.; Huang, Y.-S.; Suenaga, K. Visualization and Quantification of Transition Metal Atomic Mixing in Mo_{1-x}W_xS₂ Single Layers. *Nat. Commun.* **2013**, *4*, 1351.
- (79) Park, H. J.; Ryu, G. H.; Lee, Z. Hole Defects on Two-Dimensional Materials Formed by Electron Beam Irradiation: Toward Nanopore Devices. *Appl. Microsc.* **2015**, *45*, 107–114.
- (80) Komsa, H. P.; Kotakoski, J.; Kurasch, S.; Lehtinen, O.; Kaiser, U.; Krasheninnikov, A. V. Two-Dimensional Transition Metal Dichalcogenides Under Electron Irradiation: Defect Production and Doping. *Phys. Rev. Lett.* **2012**, *109*, 035503.
- (81) Perdew, J. P.; Burke, K.; Ernzerhof, M. Generalized Gradient Approximation Made Simple. *Phys. Rev. Lett.* **1996**, *77*, 3865–3868.
- (82) Lin, J.; Cretu, O.; Zhou, W.; Suenaga, K.; Prasai, D.; Bolotin, K. I.; Cuong, N. T.; Otani, M.; Okada, S.; Lupini, A. R.; Idrobo, J.-C.; Caudel, D.; Burger, A.; Ghimire, N. J.; Yan, J.; Mandrus, D. G.; Pennycook, S. J.; Pantelides, S. T. Flexible Metallic Nanowires with Self-Adaptive Contacts to Semiconducting Transition-Metal Dichalcogenide Monolayers. *Nat. Nanotechnol.* **2014**, *9*, 436–442.
- (83) Lin, J.; Zhang, Y.; Zhou, W.; Pantelides, S. T. Structural Flexibility and Alloying in Ultrathin Transition-Metal Chalcogenide Nanowires. *ACS Nano* **2016**, *10*, 2782–2790.
- (84) Sang, X.; Li, X.; Zhao, W.; Dong, J.; Rouleau, C. M.; Geoghegan, D. B.; Ding, F.; Xiao, K.; Unocic, R. R. *In Situ* Edge Engineering in Two-Dimensional Transition Metal Dichalcogenides. *Nat. Commun.* **2018**, *9*, 2051.
- (85) Zhou, W.; Zou, X.; Najmaei, S.; Liu, Z.; Shi, Y.; Kong, J.; Lou, J.; Ajayan, P. M.; Yakobson, B. I.; Idrobo, J.-C. Intrinsic Structural

Defects in Monolayer Molybdenum Disulfide. *Nano Lett.* **2013**, *13*, 2615–2622.

(86) Yu, Z.; Pan, Y.; Shen, Y.; Wang, Z.; Ong, Z.; Xu, T.; Xin, R.; Pan, L.; Wang, B.; Sun, L.; Wang, J.; Zhang, G.; Zhang, Y. W.; Shi, Y.; Wang, X. Towards Intrinsic Charge Transport in Monolayer Molybdenum Disulfide by Defect and Interface Engineering. *Nat. Commun.* **2014**, *5*, 5290.

(87) Qiu, H.; Xu, T.; Wang, Z.; Ren, W.; Nan, H.; Ni, Z.; Chen, Q.; Yuan, S.; Miao, F.; Song, F.; Long, G.; Shi, Y.; Sun, L.; Wang, J.; Wang, X. Hopping Transport Through Defect-Induced Localized States in Molybdenum Disulfide. *Nat. Commun.* **2013**, *4*, 2642.

(88) Barja, S.; Refaely-Abramson, S.; Schuler, B.; Qiu, D. Y.; Wickenburg, S.; Ryu, H.; Ugeda, M. M.; Kastl, C.; Chen, C.; Hwang, C.; Schwartzberg, A.; Aloni, S.; Mo, S.-K.; Ogletree, D. F.; Crommie, M. F.; Yazyev, O. V.; Louie, S. G.; Neaton, J. B.; Weber-Bargioni, A. Identifying Substitutional Oxygen as a Prolific Point Defect in Monolayer Transition Metal Dichalcogenides with Experiment and Theory. *arXiv:1810.03364*, **2018**.

(89) Zhou, S.; Wang, S.; Li, H.; Xu, W.; Gong, C.; Grossman, C.; Warner, J. H. Atomic Structure and Dynamics of Defects in 2D MoS₂ Bilayers. *ACS Omega* **2017**, *2*, 3315–3324.

(90) Hong, J.; Hu, Z.; Probert, M.; Li, K.; Lv, D.; Yang, X.; Gu, L.; Mao, N.; Feng, Q.; Xie, L.; Zhang, J.; Wu, D.; Zhang, Z.; Jin, C.; Ji, W.; Zhang, X.; Yuan, J.; Zhang, Z. Exploring Atomic Defects in Molybdenum Disulfide Monolayers. *Nat. Commun.* **2015**, *6*, 6293.

(91) Lee, Y.; Park, S.; Kim, H.; Han, G. H.; Lee, Y. H.; Kim, J. Characterization of the Structural Defects in CVD-Grown Monolayered MoS₂ Using Near-Field Photoluminescence Imaging. *Nanoscale* **2015**, *7* (28), 11909–11914.

(92) Kim, M. S.; Yun, S. J.; Lee, Y.; Seo, C.; Han, G. H.; Kim, K. K.; Lee, Y. H.; Kim, J. Biexciton Emission from Edges and Grain Boundaries of Triangular WS₂ Monolayers. *ACS Nano* **2016**, *10*, 2399–2405.

(93) Gutierrez, H. R.; Perea-López, N.; Elías, A. L.; Berkdemir, A.; Wang, B.; Lv, R.; López-Urías, F.; Crespi, V. H.; Terrones, H.; Terrones, M. Extraordinary Room-Temperature Photoluminescence in Triangular WS₂ Monolayers. *Nano Lett.* **2013**, *13*, 3447–3454.

(94) He, Z.; Wang, X.; Xu, W.; Zhou, Y.; Sheng, Y.; Rong, Y.; Smith, J. M.; Warner, J. H. Revealing Defect-State Photoluminescence in Monolayer WS₂ by Cryogenic Laser Processing. *ACS Nano* **2016**, *10*, 5847–5855.

(95) Mos, S.; Thiruraman, J. P.; Fujisawa, K.; Danda, G.; Das, P. M.; Zhang, T.; Bolotsky, A.; Terrones, M.; Drndic, M. Angstrom-Size Defect Creation and Ionic Transport Through Pores in Single-Layer MoS₂. *Nano Lett.* **2018**, *18*, 1651–1659.

(96) Lin, Y.-C.; Li, S.; Komsa, H.-P.; Chang, L.-J.; Krasheninnikov, A. V.; Eda, G.; Suenaga, K. Revealing the Atomic Defects of WS₂ Governing Its Distinct Optical Emissions. *Adv. Funct. Mater.* **2018**, *28*, 1704210.

(97) Edelberg, D.; Rhodes, D.; Kerelsky, A.; Kim, B.; Wang, J.; Zangiabadi, A.; Kim, C.; Abhinandan, A.; Scully, M.; Scullion, D.; Embon, L.; Zhang, I.; Zu, R.; Santos, E. J. G.; Balicas, L.; Marianetti, C.; Barmak, K.; Zhu, X.-Y.; Hone, J.; Pasupathy, A. N. Hundredfold Enhancement of Light Emission via Defect Control in Monolayer Transition-Metal Dichalcogenides. *arXiv:1805.00127*, **2018**.

(98) Lin, J.; Zhou, J.; Zuluaga, S.; Yu, P.; Gu, M.; Liu, Z.; Pantelides, S. T.; Suenaga, K. Anisotropic Ordering in 1T' Molybdenum and Tungsten Ditelluride Layers Alloyed with Sulfur and Selenium. *ACS Nano* **2018**, *12*, 894–901.

(99) Bampoulis, P.; Sotthewes, K.; Siekman, M. H.; Zandvliet, H. J. W. Local Conduction in Mo_xW_{1-x}Se₂: The Role of Stacking Faults, Defects, and Alloying. *ACS Appl. Mater. Interfaces* **2018**, *10*, 13218–13225.

(100) Barth, J. V.; Costantini, G.; Kern, K. Engineering Atomic and Molecular Nanostructures at Surfaces. *Nature* **2005**, *437*, 671–679.

(101) Janev, R. K. Interaction of Atomic Particles with a Solid Surface. I. Resonance Processes. *J. Phys. B: At. Mol. Phys.* **1974**, *7*, 1506–1518.

(102) Li, H.; Liu, H.; Zhou, L.; Wu, X.; Pan, Y.; Ji, W.; Zheng, B.; Zhang, Q.; Zhuang, X.; Zhu, X.; Wang, X.; Duan, X.; Pan, A. Strain-Tuning Atomic Substitution in Two-Dimensional Atomic Crystals. *ACS Nano* **2018**, *12*, 4853–4860.

(103) Zhou, W.; Zou, X.; Najmaei, S.; Liu, Z.; Shi, Y.; Kong, J.; Lou, J.; Ajayan, P. M.; Yakobson, B. I.; Idrobo, J. C. Intrinsic Structural Defects in Monolayer Molybdenum Disulfide. *Nano Lett.* **2013**, *13*, 2615–2622.

(104) Guo, Y.; Liu, D.; Robertson, J. Chalcogen Vacancies in Monolayer Transition Metal Dichalcogenides and Fermi Level Pinning at Contacts Chalcogen Vacancies in Monolayer Transition Metal Dichalcogenides and Fermi Level Pinning at Contacts. *Appl. Phys. Lett.* **2015**, *106*, 173106.

(105) Liu, D.; Guo, Y.; Fang, L.; Robertson, J. Sulfur Vacancies in Monolayer MoS₂ and Its Electrical Contacts. *Appl. Phys. Lett.* **2013**, *103*, 183113.

(106) Lin, Y. C.; Björkman, T.; Komsa, H. P.; Teng, P. Y.; Yeh, C. H.; Huang, F. S.; Lin, K. H.; Jadcak, J.; Huang, Y. S.; Chiu, P. W.; Krasheninnikov, A. V.; Suenaga, K. Three-Fold Rotational Defects in Two-Dimensional Transition Metal Dichalcogenides. *Nat. Commun.* **2015**, *6*, 6736.

(107) Liu, Z.; Suenaga, K.; Wang, Z.; Shi, Z.; Okunishi, E.; Iijima, S. Identification of Active Atomic Defects in a Monolayered Tungsten Disulfide Nanoribbon. *Nat. Commun.* **2011**, *2*, 213.

(108) Komsa, H. P.; Kurasch, S.; Lehtinen, O.; Kaiser, U.; Krasheninnikov, A. V. From Point to Extended Defects in Two-Dimensional MoS₂: Evolution of Atomic Structure Under Electron Irradiation. *Phys. Rev. B: Condens. Matter Mater. Phys.* **2013**, *88*, 035301.

(109) Zou, X.; Liu, Y.; Yakobson, B. I. Predicting Dislocations and Grain Boundaries in Two-Dimensional Metal-Disulfides from the First Principles. *Nano Lett.* **2013**, *13*, 253–258.

(110) Wood, J. D.; Schmucker, S. W.; Lyons, A. S.; Pop, E.; Lyding, J. W. Effects of Polycrystalline Cu Substrate on Graphene Growth by Chemical Vapor Deposition. *Nano Lett.* **2011**, *11*, 4547–4554.

(111) Biró, L.; Lambin, P. Grain Boundaries in Graphene Grown by Chemical Vapor Deposition. *New J. Phys.* **2013**, *15*, 035024.

(112) Yu, Q.; Jauregui, L. A.; Wu, W.; Colby, R.; Tian, J.; Su, Z.; Cao, H.; Liu, Z.; Pandey, D.; Wei, D.; Chung, T. F.; Peng, P.; Guisinger, N. P.; Stach, E. A.; Bao, J.; Pei, S.-S.; Chen, Y. P. Control and Characterization of Individual Grains and Grain Boundaries in Graphene Grown by Chemical Vapor Deposition. *Nat. Mater.* **2011**, *10*, 443–449.

(113) Greuter, F.; Blatter, G. Electrical Properties of Grain Boundaries in Polycrystalline Compound Semiconductors. *Semicond. Sci. Technol.* **1990**, *5*, 111–137.

(114) Blatter, G.; Greuter, F. Carrier Transport Through Grain Boundaries in Semiconductors. *Phys. Rev. B: Condens. Matter Mater. Phys.* **1986**, *33*, 3952–3966.

(115) Zhou, S.; Wang, S.; Shi, Z.; Sawada, H.; Kirkland, A. I.; Li, J.; Warner, J. H. Atomically Sharp Interlayer Stacking Shifts at Anti-Phase Grain Boundaries in Overlapping MoS₂ Secondary Layers. *Nanoscale* **2018**, *10*, 16692–16702.

(116) Ly, T. H.; Perello, D. J.; Zhao, J.; Deng, Q.; Kim, H.; Han, G. H.; Chae, S. H.; Jeong, H. Y.; Lee, Y. H. Misorientation-Angle-Dependent Electrical Transport Across Molybdenum Disulfide Grain Boundaries. *Nat. Commun.* **2016**, *7*, 1–7.

(117) van der Zande, A. M.; Huang, P. Y.; Chenet, D. A.; Berkelbach, T. C.; You, Y.; Lee, G.-H.; Heinz, T. F.; Reichman, D. R.; Muller, D. A.; Hone, J. C. Grains and Grain Boundaries in Highly Crystalline Monolayer Molybdenum Disulfide. *Nat. Mater.* **2013**, *12*, 554–561.

(118) Zhang, Z.; Zou, X.; Crespi, V. H.; Yakobson, B. I. Intrinsic Magnetism of Grain Boundaries in Two-Dimensional Metal Dichalcogenides. *ACS Nano* **2013**, *7*, 10475–10481.

(119) Gutiérrez, H. R.; Perea-López, N.; Elías, A. L.; Berkdemir, A.; Wang, B.; Lv, R.; López-Urías, F.; Crespi, V. H.; Terrones, H.; Terrones, M. Extraordinary Room-Temperature Photoluminescence in Triangular WS₂ Monolayers. *Nano Lett.* **2013**, *13*, 3447–3454.

- (120) Mak, K. F.; He, K.; Lee, C.; Lee, G. H.; Hone, J.; Heinz, T. F.; Shan, J. Tightly Bound Triions in Monolayer MoS₂. *Nat. Mater.* **2013**, *12*, 207–211.
- (121) Najmaei, S.; Liu, Z.; Zhou, W.; Zou, X.; Shi, G.; Lei, S.; Yakobson, B. I.; Idrobo, J.-C.; Ajayan, P. M.; Lou, J. Vapour Phase Growth and Grain Boundary Structure of Molybdenum Disulphide Atomic Layers. *Nat. Mater.* **2013**, *12*, 754–759.
- (122) Azizi, A.; Zou, X.; Ercius, P.; Zhang, Z.; Elías, A. L.; Perea-López, N.; Stone, G.; Terrones, M.; Yakobson, B. I.; Alem, N. Dislocation Motion and Grain Boundary Migration in Two-Dimensional Tungsten Disulphide. *Nat. Commun.* **2014**, *5*, 4867.
- (123) Lin, J.; Pantelides, S. T.; Zhou, W. Vacancy-Induced Formation and Growth of Inversion Domains in Transition-Metal Dichalcogenide Monolayer. *ACS Nano* **2015**, *9*, 5189–5197.
- (124) Zhang, Y.; Zhang, Y.; Ji, Q.; Ju, J.; Yuan, H.; Shi, J.; Gao, T.; Ma, D.; Liu, M.; Chen, Y.; Song, X.; Hwang, H. Y.; Cui, Y.; Liu, Z. Controlled Growth of High-Quality Monolayer WS₂ Layers on Sapphire and Imaging Its Grain Boundary. *ACS Nano* **2013**, *7*, 8963–8971.
- (125) Garcia, A.; Raya, A. M.; Mariscal, M. M.; Esparza, R.; Herrera, M.; Molina, S. I.; Scavell, G.; Galindo, P. L.; Jose-Yacamán, M.; Ponce, A. Analysis of Electron Beam Damage of Exfoliated MoS₂ Sheets and Quantitative HAADF-STEM Imaging. *Ultramicroscopy* **2014**, *146*, 33–38.
- (126) Voiry, D.; Mohite, A.; Chhowalla, M. Phase Engineering of Transition Metal Dichalcogenides. *Chem. Soc. Rev.* **2015**, *44*, 2702–2712.
- (127) Krasheninnikov, A. V. Electron Irradiation-Induced Defects and Phase Transformations in Two-Dimensional Transition Metal Dichalcogenides. *Microsc. Microanal.* **2018**, *24*, 1592–1593.
- (128) Lin, Y.-C.; Dumcenco, D. O.; Huang, Y.-S.; Suenaga, K. Atomic Mechanism of the Semiconducting-to-Metallic Phase Transition in Single-Layered MoS₂. *Nat. Nanotechnol.* **2014**, *9*, 391–396.
- (129) Zhao, J.; Deng, Q.; Bachmatiuk, A.; Sandeep, G.; Popov, A.; Eckert, J.; Rummeli, M. H. Free-Standing Single-Atom-Thick Iron Membranes Suspended in Graphene Pores. *Science* **2014**, *343*, 1228–1232.
- (130) Quang, H. T.; Bachmatiuk, A.; Dianat, A.; Ortmann, F.; Zhao, J.; Warner, J. H.; Eckert, J.; Cunniberti, G.; Rummeli, M. H. *In Situ* Observations of Free-Standing Graphene-Like Mono- and Bilayer ZnO Membranes. *ACS Nano* **2015**, *9*, 11408–11413.
- (131) Duan, X.; Wang, C.; Shaw, J. C.; Cheng, R.; Chen, Y.; Li, H.; Wu, X.; Tang, Y.; Zhang, Q.; Pan, A.; Jiang, J.; Yu, R.; Huang, Y.; Duan, X. Lateral Epitaxial Growth of Two-Dimensional Layered Semiconductor Heterojunctions. *Nat. Nanotechnol.* **2014**, *9*, 1024–1030.
- (132) Zhang, T.; Jiang, B.; Xu, Z.; Mendes, R. G.; Xiao, Y.; Chen, L.; Fang, L.; Gemming, T.; Chen, S.; Rummeli, M. H.; Fu, L. Twinned Growth Behaviour of Two-Dimensional Materials. *Nat. Commun.* **2016**, *7*, 13911.
- (133) Choudhary, N.; Park, J.; Hwang, J. Y.; Chung, H.-S.; Dumas, K. H.; Khondaker, S. I.; Choi, W.; Jung, Y. Centimeter Scale Patterned Growth of Vertically Stacked Few Layer Only 2D MoS₂/WS₂ Van Der Waals Heterostructure. *Sci. Rep.* **2016**, *6*, 25456.
- (134) Li, M. Y.; Chen, C. H.; Shi, Y.; Li, L. J. Heterostructures Based on Two-Dimensional Layered Materials and Their Potential Applications. *Mater. Today* **2016**, *19*, 322–335.
- (135) Fu, L.; Sun, Y.; Wu, N.; Mendes, R. G.; Chen, L.; Xu, Z.; Zhang, T.; Rummeli, M. H.; Rellinghaus, B.; Pohl, D.; Zhuang, L.; Fu, L. Direct Growth of MoS₂/h-BN Heterostructures via a Sulfide-Resistant Alloy. *ACS Nano* **2016**, *10*, 2063–2070.
- (136) Lin, Y.-C.; Lu, N.; Perea-Lopez, N.; Li, J.; Lin, Z.; Peng, X.; Lee, C. H.; Sun, C.; Calderin, L.; Browning, P. N.; Bresnehan, M. S.; Kim, M. J.; Mayer, T. S.; Terrones, M.; Robinson, J. A. Direct Synthesis of van Der Waals Solids. *ACS Nano* **2014**, *8*, 3715–3723.
- (137) Wang, Z.; Zhao, K.; Li, H.; Liu, Z.; Shi, Z.; Lu, J.; Suenaga, K.; Joung, S.-K.; Okazaki, T.; Jin, Z.; Gu, Z.; Gao, Z.; Iijima, S. Ultra-Narrow WS₂ Nanoribbons Encapsulated in Carbon Nanotubes. *J. Mater. Chem.* **2011**, *21*, 171–180.
- (138) Wang, Z.; Li, H.; Liu, Z.; Shi, Z.; Lu, J.; Suenaga, K.; Joung, S. K.; Okazaki, T.; Gu, Z.; Zhou, J.; Gao, Z.; Li, G.; Sanvito, S.; Wang, E.; Iijima, S. Mixed Low-Dimensional Nanomaterial: 2D Ultranarrow MoS₂ Inorganic Nanoribbons Encapsulated in Quasi-1D Carbon Nanotubes. *J. Am. Chem. Soc.* **2010**, *132*, 13840–13847.
- (139) Xie, Y.; Wang, Z.; Zhan, Y.; Zhang, P.; Wu, R.; Jiang, T.; Wu, S.; Wang, H.; Zhao, Y.; Nan, T.; Ma, X. Controllable Growth of Monolayer MoS₂ by Chemical Vapor Deposition via Close MoO₂ Precursor for Electrical and Optical Applications. *Nanotechnology* **2017**, *28*, 084001.
- (140) Lang, C.; Hiscock, M.; Larsen, K.; Moffat, J.; Sundaram, R. Characterization of Two-Dimensional Transition Metal Dichalcogenides in the Scanning Electron Microscope Using Energy Dispersive X-Ray Spectrometry, Electron Backscatter Diffraction, and Atomic Force Microscopy. *Appl. Microsc.* **2015**, *45*, 131–134.
- (141) Chhowalla, M.; Shin, H. S.; Eda, G.; Li, L. J.; Loh, K. P.; Zhang, H. The Chemistry of Two-Dimensional Layered Transition Metal Dichalcogenide Nanosheets. *Nat. Chem.* **2013**, *5*, 263–275.
- (142) Godin, K.; Cupo, C.; Yang, E. H. Reduction in Step Height Variation and Correcting Contrast Inversion in Dynamic AFM of WS₂ Monolayers. *Sci. Rep.* **2017**, *7*, 17798.
- (143) Ly, T. H.; Yun, S. J.; Thi, Q. H.; Zhao, J. Edge Delamination of Monolayer Transition Metal Dichalcogenides. *ACS Nano* **2017**, *11*, 7534–7541.
- (144) Zhang, H.; Huang, J.; Wang, Y.; Liu, R.; Huai, X.; Jiang, J.; Anfuso, C. Atomic Force Microscopy for Two-Dimensional Materials: A Tutorial Review. *Opt. Commun.* **2018**, *406*, 3–17.
- (145) Choi, J.; Zhang, H.; Du, H.; Choi, J. H. Understanding Solvent Effects on the Properties of Two-Dimensional Transition Metal Dichalcogenides. *ACS Appl. Mater. Interfaces* **2016**, *8*, 8864–8869.
- (146) Vancsó, P.; Magda, G. Z.; Peto, J.; Noh, J. Y.; Kim, Y. S.; Hwang, C.; Biró, L. P.; Tapasztó, L. The Intrinsic Defect Structure of Exfoliated MoS₂ Single Layers Revealed by Scanning Tunneling Microscopy. *Sci. Rep.* **2016**, *6*, 29726.
- (147) Ugeda, M. M.; Bradley, A. J.; Shi, S. F.; Da Jornada, F. H.; Zhang, Y.; Qiu, D. Y.; Ruan, W.; Mo, S. K.; Hussain, Z.; Shen, Z. X.; Wang, F.; Louie, S. G.; Crommie, M. F. Giant Bandgap Renormalization and Excitonic Effects in a Monolayer Transition Metal Dichalcogenide Semiconductor. *Nat. Mater.* **2014**, *13*, 1091–1095.
- (148) Hill, H. M.; Rigosi, A. F.; Rim, K. T.; Flynn, G. W.; Heinz, T. F. Band Alignment in MoS₂/WS₂ Transition Metal Dichalcogenide Heterostructures Probed by Scanning Tunneling Microscopy and Spectroscopy. *Nano Lett.* **2016**, *16*, 4831–4837.
- (149) Koós, A. A.; Vancsó, P.; Magda, G. Z.; Osváth, Z.; Kertész, K.; Dobrik, G.; Hwang, C.; Tapasztó, L.; Biró, L. P. STM Study of the MoS₂ Flakes Grown on Graphite: A Model System for Atomically Clean 2D Heterostructure Interfaces. *Carbon* **2016**, *105*, 408–415.
- (150) Ryder, C. R.; Wood, J. D.; Wells, S. A.; Hersam, M. C. Chemically Tailoring Semiconducting Two-Dimensional Transition Metal Dichalcogenides and Black Phosphorus. *ACS Nano* **2016**, *10*, 3900–3917.
- (151) Gao, J.; Kim, Y. D.; Liang, L.; Idrobo, J. C.; Chow, P.; Tan, J.; Li, B.; Li, L.; Sumpster, B. G.; Lu, T.; Meunier, V.; Hone, J.; Koratkar, N. Transition-Metal Substitution Doping in Synthetic Atomically Thin Semiconductors. *Adv. Mater.* **2016**, *28*, 9735–9743.
- (152) Cui, X.; Lee, G.-H.; Kim, Y. D.; Arefe, G.; Huang, P. Y.; Lee, C.-H.; Chenet, D. A.; Zhang, X.; Wang, L.; Ye, F.; Pizzocchero, F.; Jessen, B. S.; Watanabe, K.; Taniguchi, T.; Muller, D. A.; Low, T.; Kim, P.; Hone, J. Multi-Terminal Transport Measurements of MoS₂ Using a Van Der Waals Heterostructure Device Platform. *Nat. Nanotechnol.* **2015**, *10*, 534–540.
- (153) Shi, Y.; Huang, J. K.; Jin, L.; Hsu, Y. T.; Yu, S. F.; Li, L. J.; Yang, H. Y. Selective Decoration of Au Nanoparticles on Monolayer MoS₂ Single Crystals. *Sci. Rep.* **2013**, *3*, 1839.

- (154) Sarkar, D.; Xie, X.; Kang, J.; Zhang, H.; Liu, W.; Navarrete, J.; Moskovits, M.; Banerjee, K. Functionalization of Transition Metal Dichalcogenides with Metallic Nanoparticles: Implications for Doping and Gas-Sensing. *Nano Lett.* **2015**, *15*, 2852–2862.
- (155) Mouri, S.; Miyachi, Y.; Matsuda, K. Tunable Photoluminescence of Monolayer MoS₂ via Chemical Doping. *Nano Lett.* **2013**, *13*, 5944–5948.
- (156) Yang, L.; Majumdar, K.; Liu, H.; Du, Y.; Wu, H.; Hatzistergos, M.; Hung, P. Y.; Tieckelmann, R.; Tsai, W.; Hobbs, C.; Ye, P. D. Chloride Molecular Doping Technique on 2D Materials: WS₂ and MoS₂. *Nano Lett.* **2014**, *14*, 6275–6280.
- (157) Roy, S.; Choi, W.; Jeon, S.; Kim, D.; Kim, H.; Yun, S. J.; Lee, Y.; Lee, J.; Kim, Y.-M.; Kim, J. Atomic Observation of Filling Vacancies in Monolayer Transition Metal Sulfides by Chemically Sourced Sulfur Atoms. *Nano Lett.* **2018**, *18*, 4523–4530.
- (158) Zhu, Y.; Li, Y.; Arefe, G.; Burke, R. A.; Tan, C.; Hao, Y.; Liu, X.; Liu, X.; Yoo, W. J.; Dubey, M.; Lin, Q.; Hone, J. C. Monolayer Molybdenum Disulfide Transistors with Single-Atom-Thick Gates. *Nano Lett.* **2018**, *18*, 3807–3813.
- (159) Sangwan, V. K.; Lee, H.-S.; Bergeron, H.; Balla, I.; Beck, M. E.; Chen, K.-S.; Hersam, M. C. Multi-Terminal Memtransistors from Polycrystalline Monolayer Molybdenum Disulfide. *Nature* **2018**, *554*, 500–504.
- (160) Desai, S. B.; Madhvapathy, S. R.; Sachid, A. B.; Llinas, J. P.; Wang, Q.; Ahn, G. H.; Pitner, G.; Kim, M. J.; Bokor, J.; Hu, C.; Wong, H.-S. P.; Javey, A. MoS₂ Transistors with 1-Nanometer Gate Lengths. *Science* **2016**, *354*, 99–102.
- (161) Kang, K.; Xie, S.; Huang, L.; Han, Y.; Huang, P. Y.; Mak, K. F.; Kim, C.-J.; Muller, D.; Park, J. High-Mobility Three-Atom-Thick Semiconducting Films with Wafer-Scale Homogeneity. *Nature* **2015**, *520*, 656–660.
- (162) Wang, L.; Meric, I.; Huang, P. Y.; Gao, Q.; Gao, Y.; Tran, H.; Taniguchi, T.; Watanabe, K.; Campos, L. M.; Muller, D. A.; Guo, J.; Kim, P.; Hone, J.; Shepard, K. L.; Dean, C. R. One-Dimensional Electrical Contact to a Two-Dimensional Material. *Science* **2013**, *342*, 614–617.
- (163) Liu, X.; Lu, W.; Zhou, X.; Zhou, Y.; Zhang, C.; Lai, J.; Ge, S.; Sekhar, M. C.; Jia, S.; Chang, K.; Sun, D. Dynamical Anisotropic Response of Black Phosphorus under Magnetic Field. *2D Mater.* **2018**, *5*, 025010.
- (164) Franklin, A. D. Nanomaterials in Transistors: From High-Performance to Thin-Film Applications. *Science* **2015**, *349*, aab2750.
- (165) Cheng, R.; Jiang, S.; Chen, Y.; Liu, Y.; Weiss, N.; Cheng, H. C.; Wu, H.; Huang, Y.; Duan, X. Few-Layer Molybdenum Disulfide Transistors and Circuits for High-Speed Flexible Electronics. *Nat. Commun.* **2014**, *5*, 5143.
- (166) Schwierz, F.; Pezoldt, J.; Granzner, R. Two-Dimensional Materials and Their Prospects in Transistor Electronics. *Nanoscale* **2015**, *7*, 8261–8283.
- (167) Li, X.; Dong, J.; Idrobo, J. C.; Poretzky, A. A.; Rouleau, C. M.; Geohegan, D. B.; Ding, F.; Xiao, K. Edge-Controlled Growth and Etching of Two-Dimensional GaSe Monolayers. *J. Am. Chem. Soc.* **2017**, *139*, 482–491.
- (168) Ma, T.; Ren, W.; Zhang, X.; Liu, Z.; Gao, Y.; Yin, L.-C.; Ma, X.-L.; Ding, F.; Cheng, H.-M. Edge-Controlled Growth and Kinetics of Single-Crystal Graphene Domains by Chemical Vapor Deposition. *Proc. Natl. Acad. Sci. U. S. A.* **2013**, *110*, 20386–20391.
- (169) Liu, Y.; Dobrinsky, A.; Yakobson, B. I. Graphene Edge from Armchair to Zigzag: The Origins of Nanotube Chirality? *Phys. Rev. Lett.* **2010**, *105*, 235502.
- (170) Chen, Q.; Li, H.; Zhou, S.; Xu, W.; Chen, J.; Sawada, H.; Allen, C. S.; Kirkland, A. I.; Grossman, C.; Warner, J. H. Ultralong 1D Vacancy Channels for Rapid Atomic Migration during 2D Void Formation in Monolayer MoS₂. *ACS Nano* **2018**, *12*, 7721–7730.
- (171) Wang, S.; Robertson, A.; Warner, J. H. Atomic Structure of Defects and Dopants in 2D Layered Transition Metal Dichalcogenides. *Chem. Soc. Rev.* **2018**, *47*, 6764–6794.
- (172) Lu, A.; Zhu, H.; Xiao, J.; Chuu, C.; Han, Y.; Chiu, M.; Cheng, C.; Yang, C.; Wei, K.; Yang, Y.; Wang, Y.; Sokaras, D.; Nordlund, D.; Yang, P.; Muller, D. A.; Chou, M.-Y.; Zhang, X.; Li, L.-J. Janus Monolayers of Transition Metal Dichalcogenides. *Nat. Nanotechnol.* **2017**, *12*, 744–749.
- (173) Wang, S.; Li, H.; Sawada, H.; Allen, C. S.; Kirkland, A. I.; Grossman, J. C.; Warner, J. H. Atomic Structure and Formation Mechanism of Sub-Nanometer Pores in 2D Monolayer MoS₂. *Nanoscale* **2017**, *9*, 6417–6426.
- (174) Huang, W.; Wang, X.; Ji, X.; Zhang, Z.; Jin, C. *In-Situ* Fabrication of Mo₆S₆-Nanowire-Terminated Edges in Monolayer Molybdenum Disulfide. *Nano Res.* **2018**, *11*, 5849–5857.
- (175) Ahmed, B.; Ojha, A. K.; Singh, A.; Hirsch, F.; Fischer, I.; Patrice, D.; Materny, A. Well-Controlled *In-Situ* Growth of 2D WO₃ Rectangular Sheets on Reduced Graphene Oxide with Strong Photocatalytic and Antibacterial Properties. *J. Hazard. Mater.* **2018**, *347*, 266–278.
- (176) Arjmandi-Tash, H.; Han, Z.; Bouchiat, V. *In-Situ* Growth of Graphene on Hexagonal Boron Nitride for Electronic Transport Applications. *arXiv:1701.06062*, **2017**.
- (177) Kretschmer, S.; Komsa, H.-P.; Bøggild, P.; Krasheninnikov, A. V. Structural Transformations in Two-Dimensional Transition-Metal Dichalcogenide MoS₂ Under an Electron Beam: Insights from First-Principles Calculations. *J. Phys. Chem. Lett.* **2017**, *8*, 3061–3067.